

Prefrontal and lateral entorhinal neurons co-dependently learn item–outcome rules

<https://doi.org/10.1038/s41586-024-07868-1>

Received: 2 November 2023

Accepted: 23 July 2024

Published online: 21 August 2024

 Check for updates

Heechul Jun^{1,6}, Jason Y. Lee^{1,6}, Nicholas R. Bleza¹, Ayana Ichii¹, Jordan D. Donohue¹ & Kei M. Igarashi^{1,2,3,4,5}✉

The ability to learn novel items depends on brain functions that store information about items classified by their associated meanings and outcomes^{1–4}, but the underlying neural circuit mechanisms of this process remain poorly understood. Here we show that deep layers of the lateral entorhinal cortex (LEC) contain two groups of ‘item–outcome neurons’: one developing activity for rewarded items during learning, and another for punished items. As mice learned an olfactory item–outcome association, we found that the neuronal population of LEC layers 5/6 ($\text{LEC}_{\text{L5/6}}$) formed an internal map of pre-learned and novel items, classified into dichotomous rewarded versus punished groups. Neurons in the medial prefrontal cortex (mPFC), which form a bidirectional loop circuit with $\text{LEC}_{\text{L5/6}}$, developed an equivalent item–outcome rule map during learning. When $\text{LEC}_{\text{L5/6}}$ neurons were optogenetically inhibited, tangled mPFC representations of novel items failed to split into rewarded versus punished groups, impairing new learning by mice. Conversely, when mPFC neurons were inhibited, $\text{LEC}_{\text{L5/6}}$ representations of individual items were held completely separate, disrupting both learning and retrieval of associations. These results suggest that $\text{LEC}_{\text{L5/6}}$ neurons and mPFC neurons co-dependently encode item memory as a map of associated outcome rules.

The hippocampus and entorhinal cortex are critically involved in the formation of memory^{5,6}. Memory is thought to include neuronal encoding of information about ‘when’ (time memory), ‘where’ (spatial memory) and ‘what’ (object or item memory)^{7,8}. Past studies have identified neurons for spatial memory in the hippocampus⁹ and the medial entorhinal cortex¹⁰, whereas our understanding of neurons involved in item memory lags far behind. Neurons in layers 2/3 of the LEC receive sensory information from olfactory and somatosensory areas^{11–13}, exhibiting firing to surrounding objects and items that have olfactory, somatosensory and visual features^{14–17}. Using an olfactory item–outcome associative task, we have recently found that dopamine signals facilitate LEC_{L2a} fan cells for detecting novel odour cues associated with reward outcome¹⁸. However, LEC_{L2a} cells do not encode odour cues associated with punishment outcome, suggesting that the general function for classifying items by their outcome is implemented elsewhere⁴. Anatomically, information in LEC_{L2a} neurons is sent to the hippocampus^{17,19}, which then sends it back to $\text{LEC}_{\text{L5/6}}$; however, the functions of $\text{LEC}_{\text{L5/6}}$ remain unknown. To understand the general principle of item memory formation, we set out to investigate neurons in $\text{LEC}_{\text{L5/6}}$.

$\text{LEC}_{\text{L5/6}}$ cells encode outcome rules during associative learning

We recorded spike activity of neurons from $\text{LEC}_{\text{L5/6}}$ using our odour-based cue–outcome association task (Fig. 1a). In this task¹⁸, mice

used pre-learned knowledge to rapidly learn associations between novel odour cues and their outcomes. Mice were initially trained with pre-learning sessions, during which they learned to lick after odour-A for sucrose water reward and to withhold licking to avoid punishment of quinine water after odour-B. After mice learned to discriminate at more than 80% correct performance, daily associative learning sessions were tested. We first checked the maintained knowledge of mice in a short session with pre-learned odour-A and odour-B (AB-only session), then tested an ABab learning session immediately afterwards, in which odour-A, odour-B and a pair of novel odours (odour-a → sucrose, odour-b → quinine) were randomly presented. Mice performed pre-learned odours-A/B associations with a more than 90% correct rate throughout a session, while rapidly learning the new associations (odours-a/b) by trial and error within a 160-trial session (red trace, more than 80% at trial 29.0 ± 6.0 , $n = 8$ mice; Fig. 1b). Associative learning was repeatedly tested in individual mice using novel rewarded odours (odour-1, odour-3, odour-5, and so on; collectively termed odour-a) and novel punished odours (odour-2, odour-4, odour-6, and so on; termed odour-b). To record spike activities specifically from $\text{LEC}_{\text{L5/6}}$ cells, we used optogenetic-assisted cell-type-specific (‘opt-tag’) recording^{18,20} in *Rbp4*–Cre²¹ mice (Fig. 1c,d). Adeno-associated virus encoding channelrhodopsin-2 in a Cre-dependent manner (AAV-DIO-ChR2) was injected in the LEC, followed by an implantation of a recording device with tetrodes and an optic fibre (Extended Data Figs. 1–3). In the LEC, 30.8% of *Rbp4*⁺ cells were in layer 6, 68.8% in layer 5, 3.4% in layer 4 and

¹Department of Anatomy and Neurobiology, School of Medicine, University of California Irvine, Irvine, CA, USA. ²Department of Biomedical Engineering, Samueli School of Engineering, University of California Irvine, Irvine, CA, USA. ³Center for Neural Circuit Mapping, School of Medicine, University of California Irvine, Irvine, CA, USA. ⁴Center for the Neurobiology of Learning and Memory, University of California Irvine, Irvine, CA, USA. ⁵Institute for Memory Impairments and Neurological Disorders, University of California Irvine, Irvine, CA, USA. ⁶These authors contributed equally: Heechul Jun, Jason Y. Lee. ✉e-mail: kei.igarashi@uci.edu

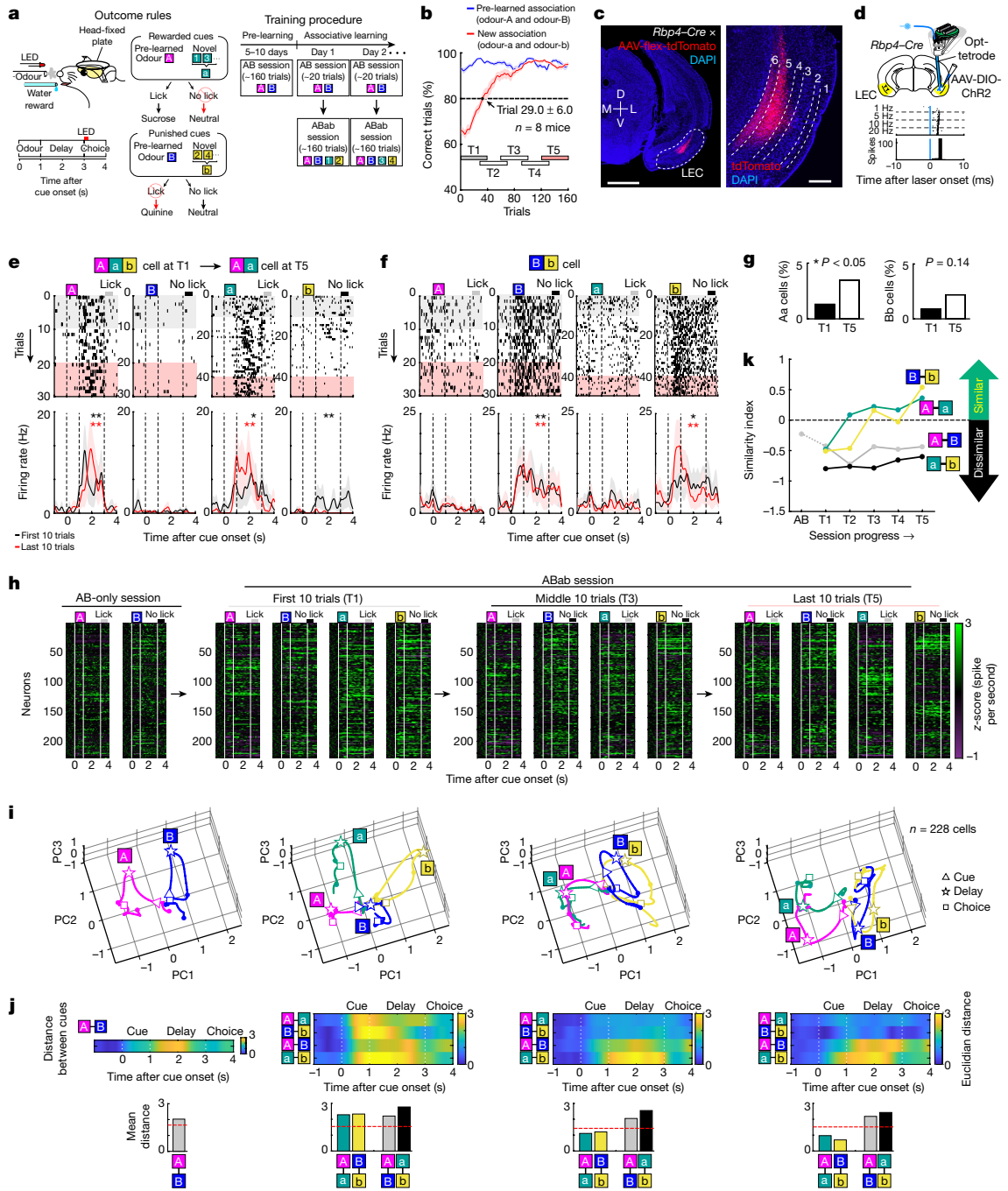


Fig. 1 See next page for caption.

3.9% in layer 3 ($n=507$ cells from 2 mice). We recorded 228 $Rbp4^+$ LEC_{L5/6} cells ($n=8$ mice) and found evolution of cue-responsive spike activity during associative learning (Fig. 1e–k). An example LEC_{L5/6} neuron (Fig. 1e) fired significantly during the cue and delay periods of odour-A (pre-learned rewarded), odour-a (novel rewarded) and odour-b (novel punished) in the initial ten trials (* $P < 0.05$ or better, rank-sum test). By the last ten trials, this cell continued to respond to odour-A, while strengthening the odour-a response (** $P < 0.01$) and losing the odour-b response ($P > 0.05$). This neuron thus changed from ‘odour-Aab cell’ to ‘odour-Aa cell’ during learning. A different example LEC_{L5/6} neuron (Fig. 1f) represents an ‘odour-Bb cell’, firing significantly to odour-B (pre-learned punished) with enhanced response to odour-b (novel punished) after learning (* $P < 0.05$ to ** $P < 0.01$). The proportion of

odour-Aa cells and odour-Bb cells showed significant and trending increases during learning, respectively ($P < 0.05$ and $P = 0.14$, binomial test), implying the role of these cells in learning (Fig. 1g).

We compared LEC_{L5/6} population activity during the AB-only session and the first, middle and last 10 trials of the ABab session (defined as timepoints 1, 3 and 5 (T1, T3 and T5), respectively; Fig. 1h and Extended Data Figs. 4 and 5). LEC_{L5/6} cells showed sustained firing from cue to delay periods, suggestive of working memory-related activity (Extended Data Fig. 4a,d). Population activity representations were then compared between each cue type using principal component analysis (PCA; Fig. 1h and Supplementary Table 5). During the AB-only session without novel cues, we observed that LEC_{L5/6} cells exhibit distinct representations between rewarded odour-A and punished odour-B, a property not

Fig. 1 | LEC_{LS/6} cells encode outcome rules during associative learning.

a, Head-fixed mice learned association between odour cues and licking for the sucrose water reward. During associative learning sessions, animals were tested with AB-only and ABab sessions with novel odours (1/2, 3/4 or 5/6, and so on). Novel odours are collectively referred to as odour-a and odour-b in subsequent figures. **b**, Correct trial rate for pre-learned odours (A/B; blue) and novel odours (a/b; red) in successful associative learning sessions. The trial number that surpassed 80% criteria (dot) and timepoints T1–T5 (rectangles) are shown. Horizontal dashed line indicates the 80% performance criteria. Data are presented as mean \pm s.e.m. **c**, Deep layer *Rbp4*⁺ cells in LEC_{LS/6} of a coronal section of a *Rbp4*-Cre mouse injected with AAV-flex-tdTomato. D, dorsal; M, medial; L, lateral; V, ventral. Scale bars, 1,000 mm (left) and 100 mm (right). **d**, Opt-tag recording of *Rbp4*⁺ cells in LEC_{LS/6}. LEC_{LS/6} cells expressing ChR2 showed a spike response to blue laser stimulation (see Methods). **e**, An example LEC_{LS/6} cell showing constant firing for odour-A and odour-a trials during an ABab associative learning session. The black trace denotes the first 10 trials. The red trace indicates the last 10 trials. This cell decreased firing for odour-b ($P = 0.042$, first 10 trials; $P = 0.63$, last 10 trials). * $P < 0.05$, ** $P < 0.01$ during the cue–delay period, two-sided signed-rank test. Data are presented as

mean \pm s.e.m. **f**, An example LEC_{LS/6} cell that developed consistent firing for odour-B and odour-b. * $P < 0.05$, ** $P < 0.01$ during the cue–delay period, two-sided signed-rank test. All data are mean \pm s.e.m. **g**, Proportion of odour-Aa-responsive (rewarded cue) and odour-Bb-responsive (punished cue) LEC_{LS/6} cells from the first 10 trials (T1) to the last 10 trials (T5). The proportion of Aa cells increased ($P = 0.011$, two-sided binomial test), whereas Bb cells showed a non-significant trend of increase ($P = 0.14$). **h**, Spike firing rate of $n = 228$ LEC_{LS/6} cells shown in the z-score during an AB-only session and the first 10 (T1), middle 10 (T3) and last 10 (T5) trials of the ABab session. **i**, Time-resolved PCA trajectory of LEC_{LS/6} cell activity for each odour type (cue onset (triangle), cue offset/delay onset (star) and delay offset (square)). **j**, Euclidian distance between odour types (top), and the mean Euclidian distance during 0.5–3.0 s after cue onset. (bottom). The 95th percentile distance obtained from shuffled data denotes significant distance (red line). **k**, Similarity index between odour-A and odour-a, odour-B and odour-b, odour-A and odour-B, and odour-a and odour-b across learning. A positive similarity index denotes similarity of representation, whereas a negative similarity index denotes dissimilarity (see main text). Horizontal dashed line indicates a border that separates similar and dissimilar representations.

observed in layer 2a fan cells¹⁸ (Fig. 1i). Upon introduction of novel cues in T1, odour-A, odour-B, odour-a and odour-b each elicited distinct representations (Fig. 1i). As learning progressed in T3, representations of novel cues became overlapped with pre-learned cues: representations for odour-A and odour-a were classified in one group, whereas those for odour-B and odour-b were classified in another. This A-a versus B-b classification was strengthened as learning progressed in T5.

To quantitatively assess the dichotomic classification of LEC_{LS/6} representation, we measured Euclidean distances between PCA trajectories (Fig. 1j). Mean distance between cue types during 0.5–3 s after cue onset was compared with a 95th-percentile distance obtained from cue-type-shuffled data¹⁸ (red line in Fig. 1j; see Methods). To evaluate the similarity between representations of each cue, we then calculated a similarity index¹⁸, where similarity index = $-(\text{distance}_{\text{real data}} - \text{distance}_{\text{shuffle}})/\text{distance}_{\text{shuffle}}$ (Fig. 1k). A positive similarity index represents significantly similar representations between two cues, whereas a negative similarity index indicates dissimilar representations. With additional timepoints T2 and T4, the similarity index plot shows that the similarity index between odour-A and odour-a and the similarity index between odour-B and odour-b were initially negative at T1 but gradually became positive during learning. This indicates that cues with the same outcomes (rewarded A-a or punished B-b) were initially represented dissimilarly but gradually became similar during learning. By contrast, cues with different outcome types (rewarded versus punished; A-B or a-b) were constantly represented dissimilarly throughout the session. A bootstrapping analysis statistically confirmed the emergence of A-a versus B-b dichotomic classification during learning (Extended Data Fig. 4h). The dichotomic classification of LEC_{LS/6} cells was also observed when incorrect trials were excluded from the PCA, excluding the possibility that the representations emerged from the increasing rate of correct trials (Extended Data Fig. 6a). Another PCA using only licking trials (correct trials for odours-A/a and error trials for odours-B/b) revealed a similar dichotomic classification, suggesting that this representation did not simply derive from lick versus no-lick motor coding (Extended Data Fig. 6b). The dichotomic classification disappeared when odour-Aa cells and odour-Bb cells were excluded from the PCA, suggesting the contribution of these neurons to the generation of the population representation (Extended Data Fig. 7a). As the opt-tagged *Rbp4*⁺ population included not only wide-spike neurons (77%, $n = 176$) but also narrow-spike neurons that might include interneurons (23%, $n = 52$), we divided recorded neurons into wide-spike and narrow-spike subpopulations and ran PCA separately (Extended Data Fig. 8a). The results showed that the dichotomic classification was observed in both populations, suggesting that both subpopulations contribute to the representation.

In sessions in which mice spontaneously did not learn new associations ('error sessions'), the dichotomic classification was lost ($n = 72$ cells; Extended Data Fig. 9), implying the role of LEC_{LS/6} cell representation in correct learning. Odour-Aa and odour-Bb cells totally disappeared in error sessions (Extended Data Fig. 9f), presumably causing the disappearance of the dichotomic classification. Together, these results demonstrate that LEC_{LS/6} cells gradually classified and grouped odour cues according to their associated outcomes during learning, suggesting their role in representing outcome rules (A/a \rightarrow rewarded versus B/b \rightarrow punished).

mPFC cells encode outcome rules concurrently with LEC_{LS/6} during associative learning

We next asked how the outcome rule information of LEC_{LS/6} cells is utilized in their target region. Previous tracing studies have shown that LEC neurons form extensive bidirectional connections with olfactory and frontal cortical regions^{22–24}. To specifically identify the output circuit of LEC_{LS/6} cells, we traced their axons in *Rbp4*-Cre mice injected with AAV-flex-tdTomato (Fig. 2a). LEC_{LS/6} axons project massively to superficial layers of the mPFC areas, including the prelimbic, infralimbic and dorsal peduncular cortices. To identify back projections from mPFC neurons to the LEC, we injected retrograde AAV-Cre in the LEC and AAV-flex-GFP in the mPFC of wild-type (WT) mice (Fig. 2b). The results showed that neurons in the prelimbic cortex project to the LEC, specifically within layers 5 and 6. These results indicate that LEC_{LS/6} and the prelimbic cortex of the mPFC have bidirectional connections.

We then recorded mPFC cells during associative learning using a recording device with independently movable tetrodes²⁵ in WT mice (Fig. 2c). Representative mPFC cells showed plastic changes in firing during learning similar to the LEC_{LS/6} cells (Fig. 2d,e and Extended Data Fig. 10). An example mPFC cell changed its tuning from odour-A cell to odour-Aa cell (Fig. 2d), whereas another mPFC cell changed from odour-B cell to odour-Bb cell (Fig. 2e). The proportion of both Aa and Bb cells increased significantly during learning (Fig. 2f, $P < 0.001$, binomial test). We performed PCA over 779 mPFC cells recorded from 6 mice (Fig. 2g,h). Similar to LEC_{LS/6} cells, mPFC cells showed separate representations for pre-learned cues with different outcome types (odour-A versus odour-B) beginning from the AB-only session and throughout the ABab session (Fig. 2h–j). By contrast, the mPFC represented novel cues (odour-a and odour-b) similarly at T1, a property not observed in the LEC_{LS/6} population. As mice learned the association, these new cues were dissociated and grouped either with odour-A (rewarded group) or odour-B (punished group) at T3–T5, as observed for the LEC_{LS/6} representations. The grouping of rewarded cues (A and a) emerged

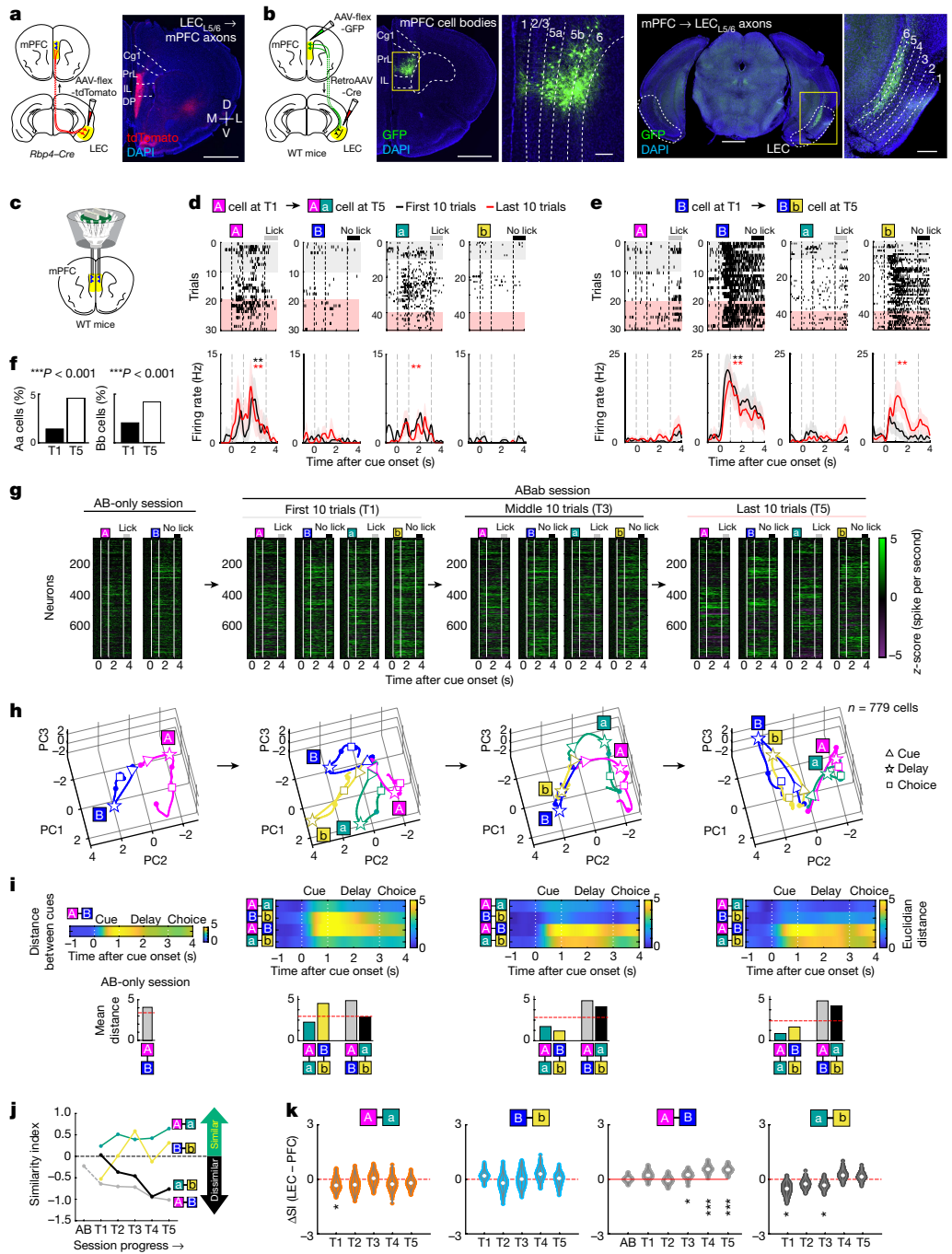


Fig. 2 | See next page for caption.

very early, beginning at the second half of T1 (Extended Data Fig. 11). Additional analyses including bootstrapping analysis (Extended Data Fig. 10h), error-exclusion analysis (Extended Data Fig. 12a), movement analysis (Extended Data Fig. 12b) and error analysis (Extended Data Fig. 13) all supported the emergence of dichotomous classification in the mPFC representation. We further compared the degree of dichotomous classification between LEC_{L5/6} and mPFC populations (Fig. 2k). A bootstrapping comparison of similarity index values showed that mPFC cells have more distinct representations for pre-learned odour-A versus odour-B after learning (T3–T5), whereas mPFC cells have more similar representations for novel cues (odour-a and odour-b) in the early phases of learning (T1–T3) than LEC_{L5/6} cells. These results suggest that mPFC cells have more clearly separated representations for learned cues associated with distinct outcomes than LEC_{L5/6} cells.

LEC_{L5/6} inhibition impaired mPFC outcome rules and new learning by mice

The LEC_{L5/6}–mPFC bidirectional circuit and their distributed outcome rule representations raised a question of how these representations are generated in this circuit. We initially tested the effect of optogenetic inhibition of LEC_{L5/6} cells. We injected AAV-flex-Jaws in the LEC of *Rbp4-Cre* mice, followed by bilateral implantation of optic fibres targeting the LEC_{L5/6} (Fig. 3a). When LEC_{L5/6} cells were inhibited with red laser, mice could not learn new associations (odours-a/b; $P < 0.001$, analysis of variance (ANOVA); $P < 0.001$, post-hoc Tukey test; $n = 10$ mice; Fig. 3b and Extended Data Figs. 14a and 15). The percentage of correct learning sessions also decreased with inhibition ($P < 0.01$, binomial test). By contrast, performance for pre-learned association (odours-A/B) was spared

Article

Fig. 2 | mPFC cells encode outcome rules concurrently with LEC_{L5/6} cells during associative learning. **a**, LEC_{L5/6} to mPFC projection. AAV-flex-tdTomato was injected unilaterally into LEC_{L5/6} of *Rbp4-Cre* mice. Axons projected to the superficial prelimbic (PrL), infralimbic (IL) and dorsal peduncular (DP) cortices. Cg1, anterior cingulate cortex. Scale bar, 1,000 mm. **b**, To identify back-projections from mPFC neurons to the LEC, retrograde AAV-Cre was injected in the LEC and AAV-flex-GFP in the mPFC of WT mice. mPFC neurons spanning across layers projected to the LEC, specifically within layers 5/6. Scale bars, 1,000 mm (first and third panels) and 100 mm (second and fourth panels). **c**, Bilateral recording of the mPFC in WT mice with an independently movable tetrode drive. **d**, An example mPFC cell showing constant firing for odour-A trials. The black trace denotes the first 10 trials. The red trace indicates the last 10 trials. This cell maintained firing for odour-a ($P = 0.045$, first 10 trials; $P = 0.045$, last 10 trials; and $**P = 0.008$ during the cue–delay period, two-sided signed-rank test). Data are presented as mean \pm s.e.m. **e**, An example mPFC cell showing constant firing for odour-B trials ($P = 0.028$, first 10 trials; and $P = 0.024$, last 10 trials) and an increase in firing for odour-b ($P = 0.09$, first 10 trials; $*P < 0.05$ and $**P < 0.01$ during the cue–delay period, two-sided signed-rank test). All data are mean \pm s.e.m. **f**, Proportion of odour-Aa-responsive (rewarded cue) and odour-Bb-responsive (punished cue) mPFC cells from the first 10 trials (T1) to the last 10 trials (T5). Both Aa and Bb cells increased

($***P = 3 \times 10^{-4}$, two-sided binomial test). **g**, Spike firing rate of $n = 779$ mPFC cells shown in z-score during the AB-only session and the first 10 (T1), middle 10 (T3) and last 10 (T5) trials of the ABab session. **h**, Time-resolved PCA trajectory of mPFC cell activity for each odour type (cue onset (triangle), cue offset/delay onset (star) and delay offset (square)). **i**, Euclidian distance between odour types (bottom), and the mean Euclidian distance during 0.5–3.0 s after cue onset (bottom). The 95th-percentile distance obtained from shuffled data denotes significant distance (red line). **j**, Similarity index between odour-A and odour-a, odour-B and odour-b, odour-A and odour-B, and odour-a and odour-b across learning. A positive similarity index denotes the similarity of representation, whereas a negative similarity index denotes dissimilarity (see the main text). Horizontal dashed line indicates a border that separates similar and dissimilar representations. **k**, Similarity index of LEC_{L5/6} cells and mPFC cells was compared using the bootstrapping method. The similarity index was calculated for 1,000 bootstraps (dots), then similarity indices for the LEC were subtracted by those for the mPFC. Horizontal dashed lines indicate zero values. A positive change in similarity index (ΔSI) for A–B after learning indicates more similar LEC representations than in the mPFC (that is, the mPFC has more distinct A–B representations; $P = 0.04$, 0.0002 and 3.8×10^{-5} in T3–T5, respectively). $*P < 0.05$, $**P < 0.01$, $***P < 0.001$; $n = 1,000$ bootstraps; two-sided bootstrapping test.

($P > 0.05$). Selective inhibition of mPFC-projecting LEC_{L5/6} cells using retrograde AAV-flex-Jaws produced a similar result ($P < 0.001$, ANOVA; $P < 0.001$, post-hoc Tukey test; $n = 10$ mice; Extended Data Fig. 14b–d). These results suggest a role for LEC_{L5/6} cells in the acquisition of new associations, but not in the retrieval of pre-learned associations, as was the case for LEC_{L2a} fan cells¹⁸.

We then tested the effect of LEC_{L5/6} inhibition on mPFC outcome rule representations. In addition to AAV injection and optic fibre implantations in the LEC_{L5/6}, *Rbp4-Cre* mice were implanted with a recording device in the mPFC (Fig. 3c). When LEC_{L5/6} cells were inhibited, mPFC cells failed to classify novel cues into rewarded versus punished groups (Fig. 3d–f and Extended Data Fig. 16). Curiously, dichotomic representations of pre-learned odour-A and odour-B remained with LEC_{L5/6} inhibition, implying that the mPFC maintains a representation of pre-learned memory without LEC_{L5/6} inputs. Continuously positive similarity index between odour-a and odour-b (SI_{a-b}), as well as negative SIs between odour A and odour-a (SI_{A-a}) and between odour-B and odour-b (SI_{B-b}), indicated that novel cues were represented in a third group distinct from both odour-A and odour-B throughout the session (Fig. 3f). Bootstrapping analyses confirmed that the dichotomic classification for novel cues was lost with inhibition (Extended Data Fig. 16e). Together, these results indicate that mPFC cells require inputs from LEC_{L5/6} cells for the classification of novel cues into rewarded versus punished dichotomic groups.

mPFC inhibition disrupted LEC_{L5/6} outcome rules, memory acquisition and retrieval

We next examined the role of mPFC cells. We tested the behavioural effect of mPFC inhibition by injecting AAV-synapsin promoter (hSyn)-Jaws and implanting optic fibres bilaterally in the mPFC of WT mice (Fig. 4a). With mPFC inhibition, mice could not surpass the 80% performance criteria for new associations (odours-a/b, $P < 0.001$, ANOVA; $P < 0.001$, post-hoc Tukey test; $n = 13$ mice; Fig. 4b and Extended Data Fig. 17a). Furthermore, mice showed a gradual performance decrease for the retrieval of pre-learned association (odours-A/B, control 94.3%, inhibition 81.9% at T5, $P < 0.001$). These results suggest that mPFC cells are critical not only for the acquisition but also for the retrieval of pre-learned associative memory. When mPFC terminals were inhibited in the LEC, mice exhibited impaired acquisition and a decreasing tendency for retrieval, implying the involvement of the mPFC–LEC_{L5/6} pathway in memory acquisition and retrieval ($P < 0.001$, ANOVA; $P < 0.001$ for odour-a/b, $P = 0.63$ for odour-A,

$P < 0.001$ for odour-a, post-hoc Tukey test; $n = 7$ mice; Extended Data Fig. 17b–d).

We then tested the effect of mPFC inhibition on the LEC_{L5/6} representations. LEC_{L5/6} cells were opt-tag recorded, and mPFC–LEC_{L5/6} axon terminals were specifically inhibited during ABab sessions (Fig. 4c and Extended Data Fig. 18). When mPFC terminals were inhibited, the independent representations of four odour cues, observed at T1 of no-inhibition sessions (Fig. 1i), were again present at T1, but never evolved throughout the session. Bootstrapping analyses confirmed the disappearance of the dichotomic classification during inhibition (Extended Data Fig. 18d). These results indicate that top-down inputs from the mPFC also have a critical role for the LEC_{L5/6} to establish classification of novel cues into rewarded versus punished groups.

To examine the role of outcome rule representations in associative learning, we plotted the similarity index of LEC_{L5/6} and mPFC cells pooled from all sessions as a function of learning performance (Fig. 4g). The correlation plots for LEC_{L5/6} representations showed partial correlations of learning performance only with SI_{A-a} and SI_{a-b} , suggesting limited relevance of LEC_{L5/6} representations to learning performance. By contrast, the plots for mPFC showed correlations of learning performance positively with SI_{A-a} ($P < 0.001$), as well as negatively with SI_{A-B} and SI_{a-b} ($P < 0.01$ or better). This result indicates that mice learned successfully when similar representations for the A–a pair and dissimilar representations for the a–b pair emerged, suggesting a critical role of mPFC outcome rule representations in associative learning performance. We compared the kinetics of outcome representations between LEC_{L5/6} cells and mPFC cells normalized by the development of behavioural performance (Extended Data Fig. 19). The result showed that the kinetics of SI_{A-a} in the mPFC correlates very well with the behavioural performance of mice during learning. By contrast, the development of SI_{A-a} in LEC_{L5/6} lagged behind the behavioural performance. Decoding analysis reproduced the early discrimination of novel cues in the mPFC (Extended Data Fig. 20). These results suggest that, although the mPFC and the LEC require mutual inputs for the establishment of their representations, it is most probably the mPFC neurons that drive the development of the outcome representation.

Discussion

Using *in vivo* recording of LEC_{L5/6} and mPFC cells during associative learning, we found that these cells establish spike classifications of rewarded versus punished cue groups in a mutually dependent manner. The dichotomic classification of cues depending on the outcomes

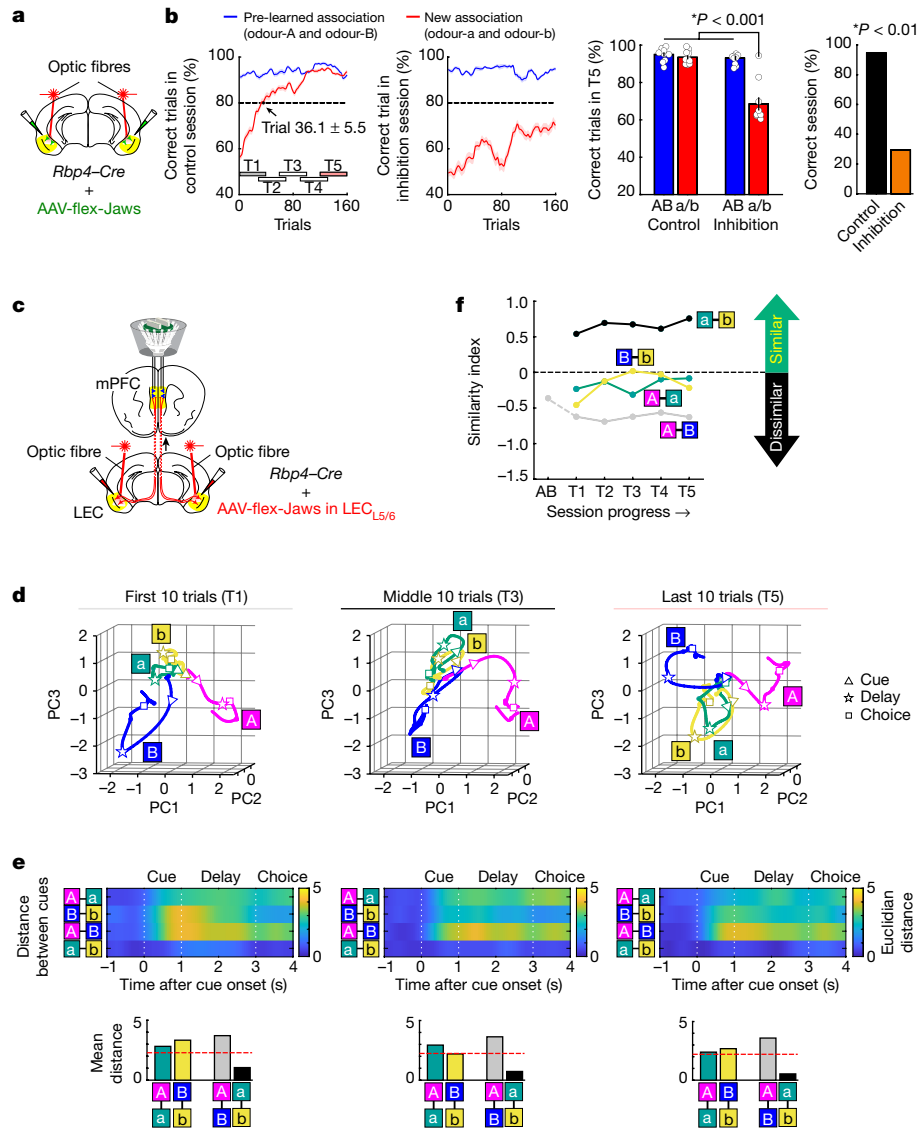


Fig. 3 | LEC_{L5/6} inhibition impairs mPFC outcome rules and new learning by mice. **a**, Optogenetic inhibition of *Rbp4*⁺ LEC_{L5/6} cells. **b**, Correct trial rate for pre-learned odours (A/B; blue) and novel odours (a/b; red) in control and inhibition sessions (left panels). The trial number that surpassed the 80% criteria (dot) and timepoints T1–T5 (rectangles) are shown. The percentage of correct trials in T5 (middle panel; $P=1.9 \times 10^{-6}$, analysis of variance (ANOVA); $P \leq 4.1 \times 10^{-9}$, post-hoc Tukey test; $n=10$ mice). The percentage of sessions in which mice correctly learned a new association (right panel; $P=5.2 \times 10^{-10}$, two-sided binomial test). Horizontal dashed line indicates the 80% performance criteria. Data are presented as mean \pm s.e.m. **c**, mPFC cells were recorded during inhibition of LEC_{L5/6} cells using optic fibres implanted bilaterally in the LEC. Jaws was expressed in the LEC of *Rbp4*-Cre mice. **d**, Trajectories of

480 mPFC cell activity at T1, T3 and T5 as in Fig. 2h, but during LEC_{L5/6} cell inhibition (cue onset (triangle), cue offset/delay onset (star) and delay offset (square)). **e**, Euclidian distance between odour types (top), and the mean Euclidian distance during 0.5–3.0 s after cue onset (bottom). The 95th-percentile distance obtained from shuffled data denotes significant distance (red line). **f**, Similarity index of the mPFC population between odour-A and odour-a, odour-B and odour-b, odour-A and odour-B, and odour-a and odour-b as in Fig. 2j, but during LEC_{L5/6} cell inhibition. A positive similarity index denotes the similarity of representation, whereas a negative similarity index denotes dissimilarity (see the main text). Horizontal dashed line indicates a border that separates similar and dissimilar representations.

(A/a \rightarrow rewarded; B/b \rightarrow punished) suggests that both regions represent learned cues using a cognitive map of non-spatial, outcome rule domains⁴. Past work in the LEC has shown its general coding of items having olfactory, somatosensory and visual features^{14–17}. Recent work has further shown reward-related representations not only for odour-cued items¹⁸ but also for spatial information²⁶ in LEC_{L2/3}. Many works on the mPFC have reported its involvement in both positive and negative outcome representations^{27–29}, although it remains unclear whether mPFC neurons represent positive and negative outcomes in dichotomous map-like representations. We propose the function of the LEC–mPFC circuit as an encoder for learned items, classifying and storing them into an outcome-based cognitive map. Whether this map can represent not

only reward versus punishment outcomes but also other dimensions of outcomes remains an intriguing question for future studies. In addition, it remains unknown which brain regions read this map, and how this map contributes to the generation of behavioural outputs. mPFC neurons make massive outputs to striatal, motor cortical and brainstem neurons involved in the generation of motor commands³⁰. Although our analyses suggested that the outcome representation did not simply derive from motor coding, our task design is an action versus no-action paradigm, and thus the outcome map may include not only information about items and outcomes but also motor-planning components.

As an underlying mechanism for the generation of this outcome map, our inhibition results underscore the critical roles of not only the

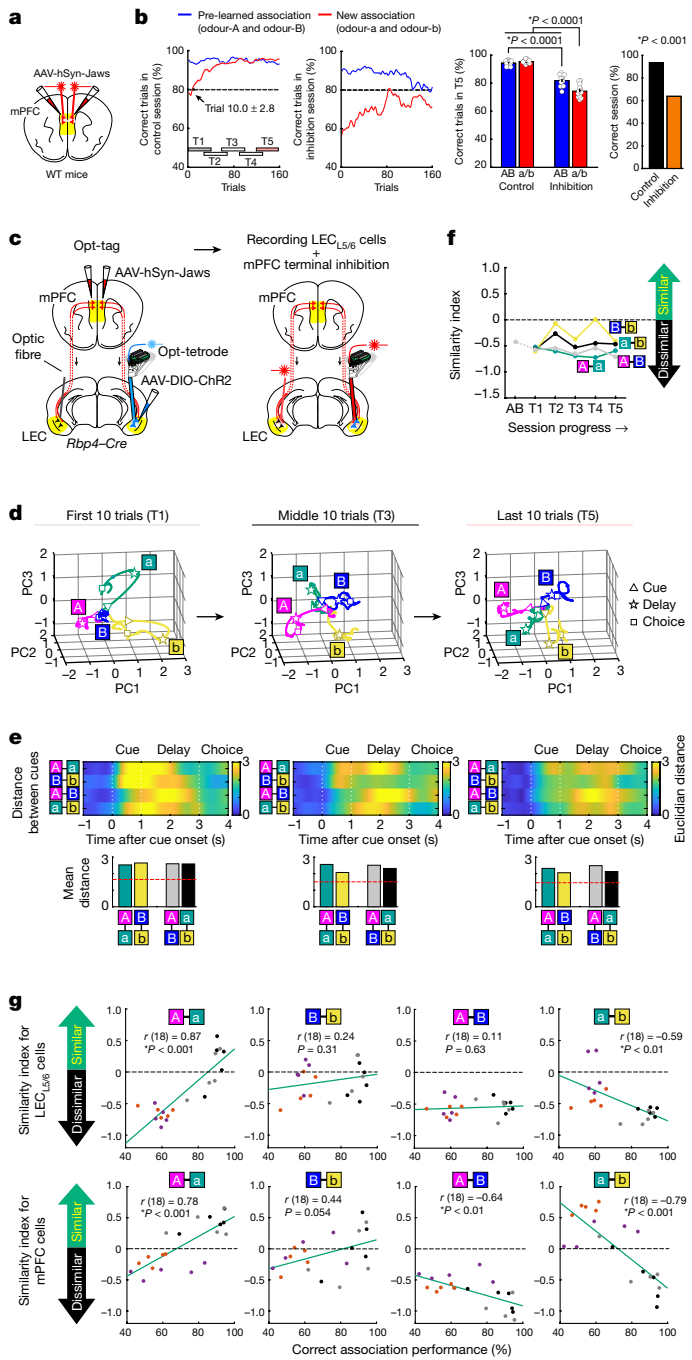


Fig. 4 | mPFC inhibition disrupts LEC_{L5/6} outcome rules, memory acquisition and retrieval. **a**, Optogenetic inhibition of mPFC cells. **b**, Correct trial rate for pre-learned odours (A/B; blue) and novel odours (a/b; red) in control and inhibition sessions (left panels). The percentage of correct trials in T5 (middle panel; $P = 1.6 \times 10^{-9}$, ANOVA; $P \leq 2.0 \times 10^{-6}$, post-hoc Tukey test; $n = 13$ mice). The percentage of sessions in which mice correctly learned a new association (right panel; $P = 2.3 \times 10^{-10}$, two-sided binomial test). Horizontal dashed line indicates the 80% performance criteria. Data are presented as mean \pm s.e.m. **c**, Opt-tag recording of LEC_{L5/6} cells was combined with inhibition of mPFC axon terminals in the LEC. Chr2 and Jaws were expressed in LEC_{L5/6} and mPFC cells, respectively, of *Rbp4-Cre* mice. **d**, Trajectories of 249 LEC_{L5/6} cell activity at T1, T3 and T5 as in Fig. 1i, but during mPFC terminal inhibition (cue onset (triangle), cue offset/delay onset (star) and delay offset (square)). **e**, Euclidian distance between odour types (top), and the mean Euclidian distance during 0.5–3.0 s after cue onset (bottom). The 95th-percentile distance obtained from shuffled data denotes significant distance (red line). **f**, Similarity index (SI) of the LEC_{L5/6} population between odour-A and odour-a, odour-B and odour-b, odour-A and odour-B, and odour-a and odour-b as in Fig. 1k, but during mPFC inhibition. A positive similarity index denotes similarity of representation, whereas a negative similarity index denotes dissimilarity (see the main text). Horizontal dashed line indicates a border that separates similar and dissimilar representations. **g**, Similarity index of LEC_{L5/6} cell representations between odours A-a, B-b, A-B and a-b as a function of associative learning performance (top). Each point represents data obtained from five timepoints (T1–T5) \times four session types (correct sessions (black) or error sessions (purple) in Fig. 1, and control sessions (grey) or mPFC inhibition sessions (orange) in Fig. 4c–f). $P = 5.4 \times 10^{-5}$ (A-a), $P = 0.63$ (B-b), $P = 0.31$ (A-B) and $P = 0.0058$ (a-b), Pearson correlation; $n = 20$ timepoints. mPFC cell representations as in the top panels are also shown (bottom). Data points are from T1–T5 \times four session types (correct sessions (black) or error sessions (purple) in Fig. 2, and control sessions (grey) or mPFC inhibition sessions (orange) in Fig. 3c–f). $P = 5.4 \times 10^{-5}$ (A-a), $P = 0.0023$ (B-b), $P = 0.054$ (A-B) and $P = 3.8 \times 10^{-5}$ (a-b), Pearson correlation; $n = 20$ timepoints. Horizontal dashed lines indicate zero values.

LEC_{L5/6}–mPFC bottom-up pathway but also the mPFC–LEC_{L5/6} top-down pathway. We presume that these two regions are part of a multilayered circuit of sensory regions \rightarrow LEC_{L2/3} \rightarrow hippocampus \rightarrow LEC_{L5/6} \hookrightarrow mPFC for the generation of item memory. In this layered circuit, LEC_{L2/3} fan cells detect novel cues associated with reward (odour-a) using dopamine inputs from the ventral tegmental area and establish the generalized representation of odour-A/a \rightarrow rewarded¹⁸. Subsequently, the hippocampus or LEC_{L5/6} may generalize punished cues and establish the representation of odour-B/b \rightarrow punished, although the precise mechanisms for generalizing punished cues remain unknown (Extended Data Fig. 21). The mPFC critically requires this outcome information from LEC_{L5/6}, and the loss of LEC_{L5/6} inputs results in the representations of novel cues in a third group, presumably a group for items that are novel but unclassified (Fig. 3).

It is intriguing to speculate what information content is transferred in the mPFC–LEC_{L5/6} top-down pathway. Computationally, this top-down

pathway would correspond to backpropagation input, which may have an important role for efficient learning in the LEC–hippocampus–mPFC multilayered network^{31,32}. Experimentally, mounting studies have demonstrated the role of the mPFC in the storage and retrieval of long-term memory^{29,33–38}. In our task, the mPFC may store outcome rules for pre-learned cues. The decreased retrieval performance for pre-learned association during mPFC inhibition (Fig. 4), contrasted by the intact mPFC representations of pre-learned cues during LEC_{L5/6} inhibition (Fig. 3) support this notion. The stored memory in the mPFC may be transferred to the LEC and hippocampus as a memory schema through LEC_{L5/6} for guiding subsequent new learning^{36,39,40}. The pre-existing distinct trajectories of rewarded odour-A and punished odour-B in the AB-only sessions imply that these representations are used as memory schema for integrating new information. With terminal inhibition of the mPFC–LEC_{L5/6} top-down pathway, the schema may not be transferred to LEC_{L5/6}, blocking the classification of odour cues into two groups (Fig. 4). During mPFC inhibition, the distinct representations of four odours in LEC_{L5/6} might derive from an intrinsic cue-dissociating property of LEC_{L5/6} cells based on olfactory sensory inputs, whereas the slow decay of the pre-learned association may be induced by compensatory activity from surrounding frontal regions.

The interactions between the mPFC and entorhinal–hippocampal memory circuit have been one of the major topics in memory research^{29,37,41,42}. Previous studies have identified unidirectional information transfer in the direct ventral hippocampus–mPFC pathway^{43,44} and the mPFC–hippocampus bidirectional indirect pathway via the thalamic nucleus reuniens⁴⁵, whereas the role of the LEC–mPFC pathway remained enigmatic as a ‘missing piece’³⁷. Our study identified the role of the LEC_{L5/6}–mPFC circuit as a coherent memory-encoding system during learning. The LEC is considered one of the few hub regions of the brain forming bidirectional connections with widespread cortical

regions, including the olfactory cortical regions, nucleus accumbens and orbitofrontal cortex²⁴. Previous work has identified reward-related and goal-related representations in the orbitofrontal cortex^{46–48}, which may work coherently with the LEC–mPFC circuit for the generation of goal-oriented behavioural outputs. Future studies that tease apart the interdependency of the LEC and its connected brain regions are expected to elucidate the distinctive roles of LEC–cortical bidirectional circuits.

Online content

Any methods, additional references, Nature Portfolio reporting summaries, source data, extended data, supplementary information, acknowledgements, peer review information; details of author contributions and competing interests; and statements of data and code availability are available at <https://doi.org/10.1038/s41586-024-07868-1>.

1. Suzuki, W. A. Associative learning signals in the brain. *Prog. Brain Res.* **169**, 305–320 (2008).
2. Osada, T., Adachi, Y., Kimura, H. M. & Miyashita, Y. Towards understanding of the cortical network underlying associative memory. *Phil. Trans. R. Soc. B* **363**, 2187–2199 (2008).
3. Ozawa, T. & Johansen, J. P. Learning rules for aversive associative memory formation. *Curr. Opin. Neurobiol.* **49**, 148–157 (2018).
4. Igarashi, K. M., Lee, J. Y. & Jun, H. Reconciling neuronal representations of schema, abstract task structure, and categorization under cognitive maps in the entorhinal–hippocampal–frontal circuits. *Curr. Opin. Neurobiol.* **77**, 102641 (2022).
5. Squire, L. R. Memory and the hippocampus: a synthesis from findings with rats, monkeys, and humans. *Psychol. Rev.* **99**, 195–231 (1992).
6. Buszaki, G. & Moser, E. I. Memory, navigation and theta rhythm in the hippocampal–entorhinal system. *Nat. Neurosci.* **16**, 130–138 (2013).
7. Morris, R. G. in *The Hippocampus Book* (ed. P. Andersen, P.) 581–714 (Oxford Univ. Press, 2007).
8. Eichenbaum, H. On the integration of space, time, and memory. *Neuron* **95**, 1007–1018 (2017).
9. O’Keefe, J. & Nadel, L. *The Hippocampus as a Cognitive Map* (Oxford Univ. Press, 1978).
10. Moser, E. I., Moser, M. B. & Roudi, Y. Network mechanisms of grid cells. *Phil. Trans. R. Soc. C* **369**, 20120511 (2014).
11. Price, J. L. An autoradiographic study of complementary laminar patterns of termination of afferent fibers to the olfactory cortex. *J. Comp. Neurol.* **150**, 87–108 (1973).
12. Burwell, R. D. The parahippocampal region: corticocortical connectivity. *Ann. N. Y. Acad. Sci.* **911**, 25–42 (2000).
13. Igarashi, K. M. et al. Parallel mitral and tufted cell pathways route distinct odor information to different targets in the olfactory cortex. *J. Neurosci.* **32**, 7970–7985 (2012).
14. Young, B. J., Otto, T., Fox, G. D. & Eichenbaum, H. Memory representation within the parahippocampal region. *J. Neurosci.* **17**, 5183–5195 (1997).
15. Deshmukh, S. S. & Knierim, J. J. Representation of non-spatial and spatial information in the lateral entorhinal cortex. *Front. Behav. Neurosci.* **5**, 69 (2011).
16. Tsao, A., Moser, M. B. & Moser, E. I. Traces of experience in the lateral entorhinal cortex. *Curr. Biol.* **23**, 399–405 (2013).
17. Igarashi, K. M., Lu, L., Colgin, L. L., Moser, M. B. & Moser, E. I. Coordination of entorhinal–hippocampal ensemble activity during associative learning. *Nature* **510**, 143–147 (2014).
18. Lee, J. Y. et al. Dopamine facilitates associative memory encoding in the entorhinal cortex. *Nature* **598**, 321–326 (2021).
19. Martin, C., Beshel, J. & Kay, L. M. An olfacto-hippocampal network is dynamically involved in odor-discrimination learning. *J. Neurophysiol.* **98**, 2196–2205 (2007).
20. Cohen, J. Y., Haesler, S., Vong, L., Lowell, B. B. & Uchida, N. Neuron-type-specific signals for reward and punishment in the ventral tegmental area. *Nature* **482**, 85–88 (2012).
21. Luo, W. et al. Acquiring new memories in neocortex of hippocampal-lesioned mice. *Nat. Commun.* **13**, 1601 (2022).
22. Insausti, R., Herrero, M. T. & Witter, M. P. Entorhinal cortex of the rat: cytoarchitectonic subdivisions and the origin and distribution of cortical efferents. *Hippocampus* **7**, 146–183 (1997).
23. Witter, M. P. & Amaral, D. G. in *The Rat Nervous System* 3rd edn (ed. Paxinos, G.) 635–704 (Elsevier, 2004).
24. Zingg, B. et al. Neural networks of the mouse neocortex. *Cell* **156**, 1096–1111 (2014).
25. Jun, H. et al. Disrupted place cell remapping and impaired grid cells in a knockin model of Alzheimer’s disease. *Neuron* **107**, 1095–1112.e6 (2020).
26. Issa, J. B., Radvansky, B. A., Xuan, F. & Dombeck, D. A. Lateral entorhinal cortex subpopulations represent experiential epochs surrounding reward. *Nat. Neurosci.* **27**, 536–546 (2024).
27. Mulder, A. B., Nordquist, R., Orgut, O. & Pennartz, C. M. Plasticity of neuronal firing in deep layers of the medial prefrontal cortex in rats engaged in operant conditioning. *Prog. Brain Res.* **126**, 287–301 (2000).
28. Rushworth, M. F., Noonan, M. P., Boorman, E. D., Walton, M. E. & Behrens, T. E. Frontal cortex and reward-guided learning and decision-making. *Neuron* **70**, 1054–1069 (2011).
29. Euston, D. R., Gruber, A. J. & McNaughton, B. L. The role of medial prefrontal cortex in memory and decision making. *Neuron* **76**, 1057–1070 (2012).
30. Anastasiades, P. G. & Carter, A. G. Circuit organization of the rodent medial prefrontal cortex. *Trends Neurosci.* **44**, 550–563 (2021).
31. Lillicrap, T. P., Santoro, A., Marris, L., Akerman, C. J. & Hinton, G. Backpropagation and the brain. *Nat. Rev. Neurosci.* **21**, 335–346 (2020).
32. Konishi, M. I., Igarashi, K. M. & Miura, K. Biologically plausible local synaptic learning rules robustly implement deep supervised learning. *Front. Neurosci.* **17**, 1160899 (2023).
33. Hasegawa, I., Fukushima, T., Ihara, T. & Miyashita, Y. Callosal window between prefrontal cortices: cognitive interaction to retrieve long-term memory. *Science* **281**, 814–818 (1998).
34. Tomita, H., Ohbayashi, M., Nakahara, K., Hasegawa, I. & Miyashita, Y. Top-down signal from prefrontal cortex in executive control of memory retrieval. *Nature* **401**, 699–703 (1999).
35. Frankland, P. W. & Bontempi, B. The organization of recent and remote memories. *Nat. Rev. Neurosci.* **6**, 119–130 (2005).
36. Tse, D. et al. Schema-dependent gene activation and memory encoding in neocortex. *Science* **333**, 891–895 (2011).
37. Eichenbaum, H. Prefrontal–hippocampal interactions in episodic memory. *Nat. Rev. Neurosci.* **18**, 547–558 (2017).
38. Kitamura, T. et al. Engrams and circuits crucial for systems consolidation of a memory. *Science* **356**, 73–78 (2017).
39. Tse, D. et al. Schemas and memory consolidation. *Science* **316**, 76–82 (2007).
40. Baraduc, P., Duhamel, J. R. & Wirth, S. Schema cells in the macaque hippocampus. *Science* **363**, 635–639 (2019).
41. Simons, J. S. & Spiers, H. J. Prefrontal and medial temporal lobe interactions in long-term memory. *Nat. Rev. Neurosci.* **4**, 637–648 (2003).
42. Ito, H. T. Prefrontal–hippocampal interactions for spatial navigation. *Neurosci. Res.* **129**, 2–7 (2018).
43. Spellman, T. et al. Hippocampal–prefrontal input supports spatial encoding in working memory. *Nature* **522**, 309–314 (2015).
44. Place, R., Farovik, A., Brockmann, M. & Eichenbaum, H. Bidirectional prefrontal–hippocampal interactions support context-guided memory. *Nat. Neurosci.* **19**, 992–994 (2016).
45. Ito, H. T., Zhang, S. J., Witter, M. P., Moser, E. I. & Moser, M. B. A prefrontal–thalamo–hippocampal circuit for goal-directed spatial coding. *Nature* <https://doi.org/10.1038/nature14396> (2015).
46. Feierstein, C. E., Quirk, M. C., Uchida, N., Sosulski, D. L. & Mainen, Z. F. Representation of spatial goals in rat orbitofrontal cortex. *Neuron* **51**, 495–507 (2006).
47. Wang, P. Y. et al. Transient and persistent representations of odor value in prefrontal cortex. *Neuron* **108**, 209–224.e6 (2020).
48. Basu, R. et al. The orbitofrontal cortex maps future navigational goals. *Nature* **599**, 449–452 (2021).

Publisher’s note Springer Nature remains neutral with regard to jurisdictional claims in published maps and institutional affiliations.

Springer Nature or its licensor (e.g. a society or other partner) holds exclusive rights to this article under a publishing agreement with the author(s) or other rightsholder(s); author self-archiving of the accepted manuscript version of this article is solely governed by the terms of such publishing agreement and applicable law.

© The Author(s), under exclusive licence to Springer Nature Limited 2024

Article

Methods

Mice

All procedures were conducted in accordance with the guidelines of the National Institutes of Health and approved by the Institutional Animal Care and Use Committee at the University of California, Irvine. Mice were maintained in standard enriched housing conditions with ambient temperature set to 23 °C and humidity to 40%, on a reversed 12 h dark-light cycle with food and water provided ad libitum. All experiments were conducted during the dark phase. Mouse lines and their received procedure are summarized in Supplementary Tables 2 and 4.

All animals either had the C57BL/6 background or were backcrossed to C57BL/6 for at least seven generations. Animals were 3–5 months old at the time of surgical procedures. They were housed individually with an exercise wheel following their first procedure. Medications and appropriate treatments were applied across 1–2 weeks for recovery. If animals died or were sick during or before the experiment, their recording positions could not be validated and therefore were removed from the data analysis. We used similar numbers of males and females, and noted no significant difference in our preliminary analyses between sexes.

Electrode, drive and optic fibre preparation

Opt-tetrode drive. Custom-built 64-channel drives featuring tetrodes bundled around an optic fibre were used for opt-tag recording as previously described¹⁸.

mPFC drive. A custom-built 64-channel drive with independently moving tetrodes for recording mPFC was used as previously described⁴⁹.

Optic fibres. For optogenetic inhibition experiments, optic fibres of 400 µm in diameter cut to 10–13 mm in length (Thorlabs) were used.

Surgery

All surgical procedures were performed as previously described^{18,49}. Mice received post-operative injections of flunixin and enrofloxacin daily as needed.

Injections. For injections targeting the LEC, a 1-mm craniotomy was centred at anteroposterior 3.5–3.7 mm and mediolateral 3.5 mm from Bregma. The injection needle was angled at 10° laterally and inserted 3.0–3.5-mm deep from the brain surface. For injections targeting the mPFC, the craniotomy was centred at anteroposterior 1.6–1.8 mm and mediolateral 0.8 mm from Bregma. The injection needle was angled at 8–10° medially and inserted 1.3–1.8-mm deep from the brain surface. Viruses were manually injected at approximately 0.1 µl min⁻¹ using a hydraulic manipulator (MO-10, Narishige). AAVs used in the study are summarized in Supplementary Table 4.

Tetrode drive and optic fibre implantations. After allowing at least 1 week recovery from injection surgeries, mice were implanted with tetrode drives or optic fibres as previously described^{18,49}. In brief, a custom titanium head-plate was affixed to the skull, then craniotomies were drilled at the LEC or mPFC coordinates described above. For drive implants, reference wire was implanted on the cerebellar surface. Drives or optic fibres were secured to the skull with dental acrylic and protected with foil-lined conical shields.

Training procedures

Behavioural training was performed as previously described¹⁸. In brief, mice were deprived of water to 85% of baseline following post-operative recovery. Mice were habituated to head fixation inside the custom sound-proof chamber for 1–4 days. Licks were detected with an infrared emitter and sensor positioned at the sucrose or quinine lick spout. Tasks were automated with custom LabView scripts on a laptop connected to

a DAQ port (National Instruments). Mice were trained to lick actively for sucrose in response to an LED cue following non-odourized air (1–5 days). They were then trained to withhold licking during the 2-s delay period between air and LED cue (1–5 days). For pre-learning of the go/no-go task, mice learned to lick for sucrose in response to Go odour-A (isoamyl acetate) and withhold licking to No-go odour B (α-pinene) to avoid quinine. Pre-learning typically took 5–10 days.

Associative learning. An approximately 20-trial session with random trials of only odour-A and odour-B was tested first (AB-only session). Immediately afterwards, two novel odours in addition to odour-A and odour-B were presented in random order every 18–22 s (ABab session). One of the novel odours was associated with lick, and the other with no-lick. Mice learned this new association by trial and error. Novel odour pairs were never repeated for an individual mouse. The lick-associated odours (odour-1, odour-3, odour-5, and so on) were collectively termed as odour-a, and the no-lick-associated odours (odour-2, odour-4, odour-6, and so on) were termed as odour-b. Odour-A and odour-B were randomly delivered with a 20% emergence rate each, whereas odour-a and odour-b were delivered with a 30% emergence rate each. Licking during the delay period automatically aborted the trial. Odours used in the study are summarized in Supplementary Table 3.

Data collection

Spike recording. Spiked data were acquired as previously described¹⁸ using Cheetah v6.1 software (Neuralynx Inc). Tetrodes were advanced 40–80 µm to record a different group of cells in each session of a same type (either control or inhibition session) at the same recording position, assuring that identical cells were not double sampled. We typically advanced tetrodes after the recording of one control session and one inhibition session. In each daily recording, two opt-tagging blocks were performed before and after the behaviour recording sessions. Five-millisecond pulses of 465-nm blue-laser stimulation (7–9 mW mm⁻² at the tip of the implanted optic fibre) were delivered through the implanted optic fibre at varying frequencies of 1–20 Hz.

Optogenetic inhibition. Optogenetic inhibition was performed as previously described¹⁸. Laser was held on from the cue onset for 5 s, followed by a linear taper of 10 s on each trial. For control experiments, we used no-laser sessions in the same mice used for inhibition¹⁸, in which disconnected laser patch fibre tips were placed inside the implanted conical shield and the laser was applied inside the shield with the same condition as inhibition sessions. We previously compared this no-laser control group and GFP-injected control group, and observed no difference between them¹⁸. To control for the unequal number of sessions from individual mice, we averaged behavioural performance across sessions for each mouse and used these mean values (see ‘Data analysis’ below).

Data analysis

Unless indicated otherwise, analyses were performed using MATLAB codes written by the authors.

Behavioural analysis. Behavioural performance was calculated as previously described¹⁸. In brief, instantaneous behavioural performance for odours-A/B and odours-a/b was calculated within a sliding window of 20 trials. The percentage of correct trials in T5 was calculated from trials 121–160. To evaluate the behavioural performance for each mouse, these two values were averaged for all sessions with the same condition (control or inhibition) for each mouse. ‘Correct’ sessions were considered as those with (percent correct trials in T5) more than 80%.

Spike sorting. Spike sorting was performed as previously described^{18,49}. Putative excitatory cells with a spike peak-valley width of more than 200 µs and cells with more than 100 spikes in a session were included

for further analysis. Double-counting cells were avoided by comparing clusters before and after tetrode turns.

Opt-tag cell identification. Putative excitatory cells that responded consistently to blue-laser pulses were tagged as *Rbp4*⁺ cells. We used the same criteria for opt-tagged neurons as previously described¹⁸. In brief, the optic response during 10 ms after the laser stimulation was statistically compared from baseline spike activity during -100 to 0 ms before the laser stimulation using Kullback–Leibler divergence (stimulus-associated spike latency test (SALT))⁵⁰. Neurons with $P < 0.01$ in SALT and waveform correlation of more than 0.85 were considered as layer 5/6 cells.

Spike response. Mean firing rates in 50-ms bins were obtained using a Gaussian filter with a sigma of 100 ms and transformed as z-score using the mean firing rate during the baseline pre-odour period (-1 to 0 s from odour onset). Significant response was assessed from total spike numbers during odour (0.5–1.5 s after odour onset), delay (2–3 s after odour onset), odour + delay (0.5–3 s after odour onset) and choice (3–4 s after odour onset) periods, compared with those in the 1-s pre-odour period (Wilcoxon signed-rank test). We used 0.5–1.5 s after odour onset for the odour response period because of the delay from odour delivery to the onset of LEC activity observed in this and previous studies (Igarashi et al.¹⁷). The delay period was chosen as a period 2–3 s after odour onset because of this delay in LEC activity.

PCA. PCA was performed as previously described¹⁸. Principal components 1–3 were used for the subsequent analyses. Euclidian distances were calculated between each odour trial type. The Euclidian distance during the odour + delay period of 0.5–3.0 s after odour onset was assessed as the mean distance between odour trial types. For percent variance explained by principal components 1–3 in main figures, see Supplementary Table 5.

Shuffle analysis. Shuffle analysis was used to statistically evaluate the mean distances between odour types^{13,18}. Shuffle data were obtained by randomly shuffling the assignment of odour type for each trial while keeping the total number of each trial type the same as the original real data. With this shuffling procedure, the distinct response to specific odour types observed in the original data disappeared, producing randomly distributed spike responses in each odour trial type. The mean distance during the 2.5-s period of 0.5–3.0 s after odour onset was obtained for each shuffled data. This procedure was repeated 1,000 times, producing 1,000 distances for each odour pair. The upper 95th percentile of 1,000 distances from each odour pair was averaged and used as a threshold for the statistical assessment.

Similarity index. A mean shuffle distance was obtained by averaging the shuffle distance across T1–T5. A similarity index (SI) was calculated as the difference between real and mean shuffled distance, normalized by the mean shuffled distance¹⁸:

$$SI = -(\text{Mean distance}_{\text{real_data}} - \text{Mean distance}_{\text{shuffle}}) / \text{Mean distance}_{\text{shuffle}}$$

The numerator of the similarity index was negatively flipped so that the similarity index becomes positive if the distance obtained from a given odour pair was smaller than the shuffle distance (similar representations of two odours), and negative if the distance was larger than the shuffle distance (dissimilar representations of two odours).

Bootstrapping analysis. The change of the similarity index during associative learning was compared using the bootstrapping method as

previously described¹⁸. In brief, PCA was performed from a resampled neuronal population, and this procedure was repeated 1,000 times to make 1,000 bootstraps. The similarity index was calculated for each bootstrap, then similarity indices in T2–T5 were subtracted by that in T1, to test for a significant distribution above or below zero. Distribution of difference with $P < 0.05$ above or below zero was considered significant. The bootstraps were also compared between control and inhibition sessions.

Histology and reconstruction of recording positions

Electrode positions. Recording positions were confirmed as previously described by passing electrical current through tetrodes in anaesthetized mice, followed by fixation in 4% paraformaldehyde and cryosectioning^{18,49}. Only data from tetrodes in the LEC_{L5/6} or mPFC were collected for analysis. Note that electrical lesions typically expanded holes in the brain sections, so that they spanned across cell layers.

Statistics and reproducibility

Data are shown with \pm standard error. The animal numbers and sampled neuron numbers (biological replicates) were designed to achieve a power of greater than 0.8. Both sexes of animals were used. For statistical testing, data were first tested for normal distribution using the Kolmogorov–Smirnov test ($P < 0.05$ cut-off). All statistical methods used are summarized in Supplementary Table 1 and were two-sided.

Histological experiments were repeated independently in different mice with similar results for Fig. 2a ($n = 6$ mice) and Fig. 2b ($n = 5$ mice).

Reporting summary

Further information on research design is available in the Nature Portfolio Reporting Summary linked to this article.

Data availability

The neurophysiological data generated in this study are available on request.

Code availability

The neurophysiological data and analytical codes are available on request and will be deposited with a subsequent protocol paper.

49. Jun, H., Chavez, J., Bramian, A. & Igarashi, K. M. Protocol for remapping of place cells in disease mouse models. *STAR Protoc.* **2**, 100759 (2021).
50. Kvitsiani, D. et al. Distinct behavioural and network correlates of two interneuron types in prefrontal cortex. *Nature* **20**, 363–366 (2013).

Acknowledgements We thank M. Witter and A. Treves, and members in the Igarashi laboratory for providing valuable comments on this work. The work was supported by the US National Institutes of Health (NIH) R01 grants (R01MH121736, R01AG063864, R01AG066806 and R01AG086441) and a BrightFocus Foundation Research grant (A2019380S) to K.M.I. H.J. was supported by the University of California, Irvine Medical Scientist Training Program (MSTP; T32GM008620) and the NIH F31 grant (F31AG069500). J.Y.L. was supported by the NIH F31 grant (F31AG074650).

Author contributions H.J., J.Y.L. and K.M.I. conceived the project and designed the experiments. H.J., J.Y.L., N.R.B., A.I. and J.D.D. performed the experiments. H.J., J.Y.L. and K.M.I. performed the analyses. H.J., J.Y.L. and K.M.I. wrote the paper with input from all authors.

Competing interests The authors declare no competing interests.

Additional information

Supplementary information The online version contains supplementary material available at <https://doi.org/10.1038/s41586-024-07868-1>.

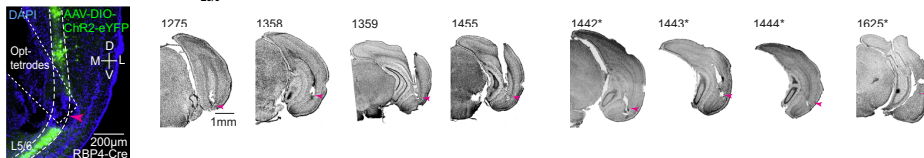
Correspondence and requests for materials should be addressed to Kei M. Igarashi.

Peer review information *Nature* thanks Thomas McHugh and the other, anonymous, reviewer(s) for their contribution to the peer review of this work.

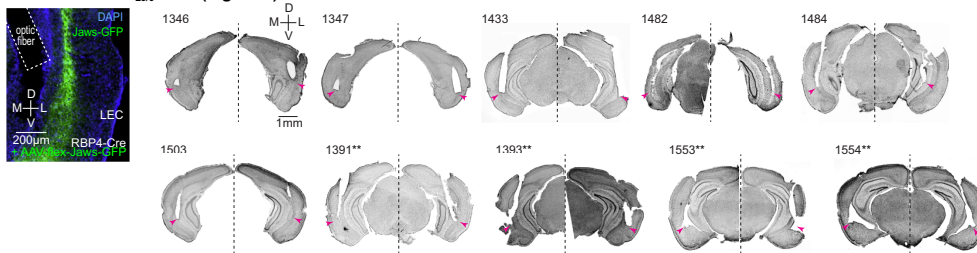
Reprints and permissions information is available at <http://www.nature.com/reprints>.

Article

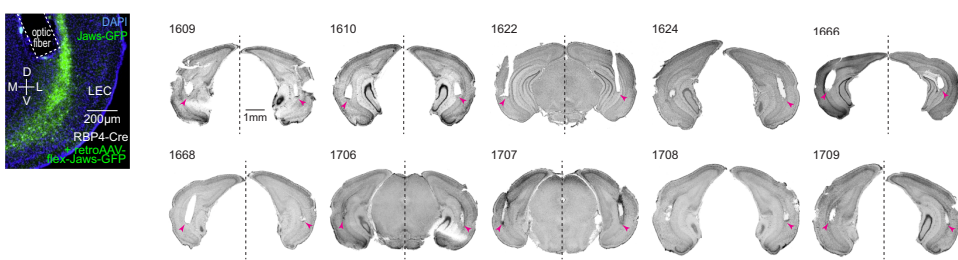
a Opt-tag recording of LEC_{L5/6} cells (Figures 1 and 4)



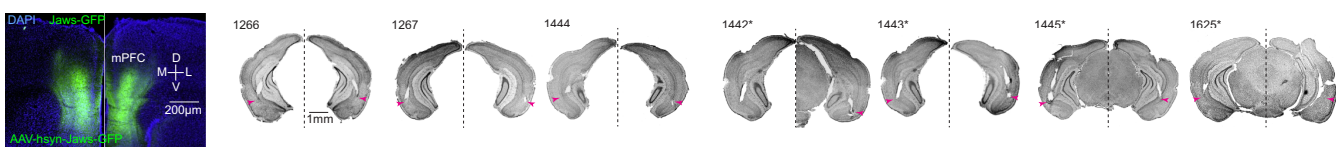
b Inhibition of LEC_{L5/6} cells (Figure 3)



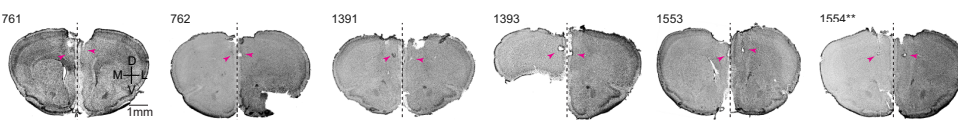
c Inhibition of mPFC-projecting LEC_{L5/6} cells (Extended Figure 8)



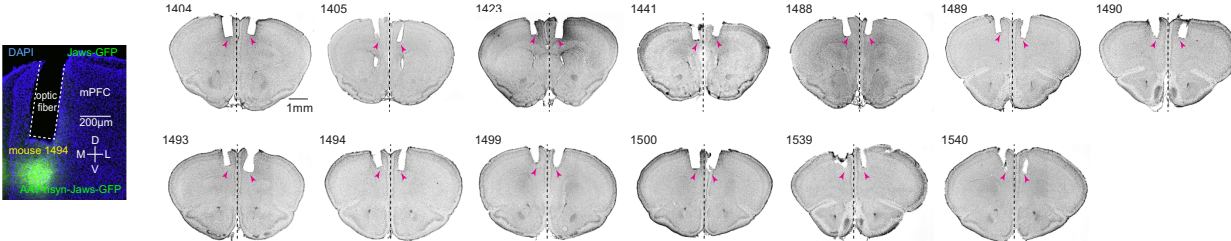
d mPFC terminal inhibition (Figure 4 and Extended Figure 10)



e Recording mPFC cells (Figure 2)



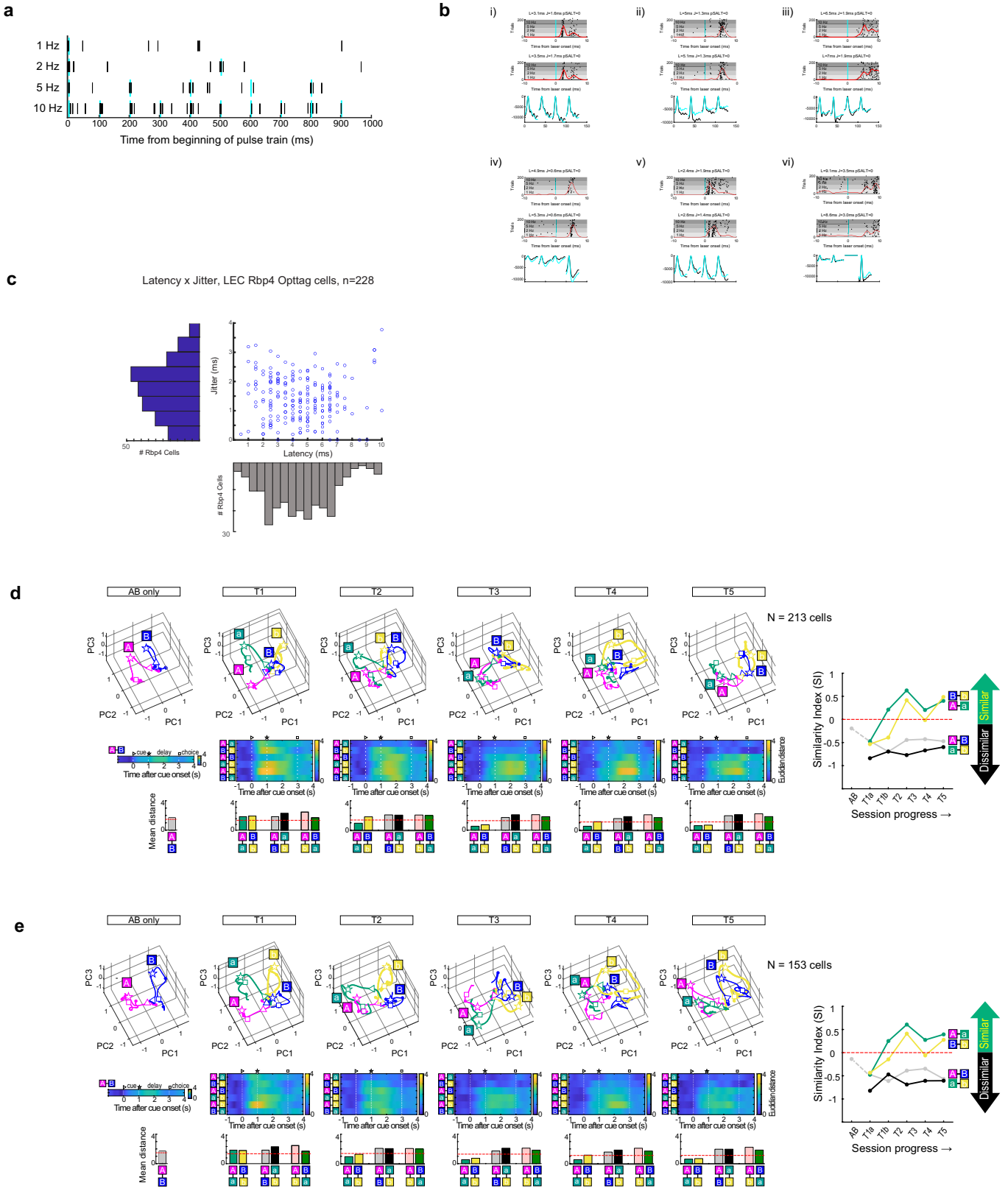
f Inhibition of mPFC cells (Figure 4)



Extended Data Fig. 1 | Histological validation of implanted sites.

(a) Recording positions in LEC of *Rbp4-Cre* mice for opt-tagging experiment (Figs. 1 and 4). Positions were marked with electrolytic lesioning. D, dorsal, V, ventral, M, medial, L, lateral. **(b)** Optic fiber positions in LEC of *Rbp4-Cre* mice injected with AAV-flex-Jaws-GFP into LEC for inhibition experiments (Fig. 3). Arrowhead, estimated tip of optic fibers. **(c)** Optic fiber positions in LEC of *Rbp4-Cre* mice injected with retroAAV-flex-Jaws-GFP into mPFC for inhibition of mPFC-projecting LEC cells (Extended Data Fig. 14). **(d)** Optic fiber positions

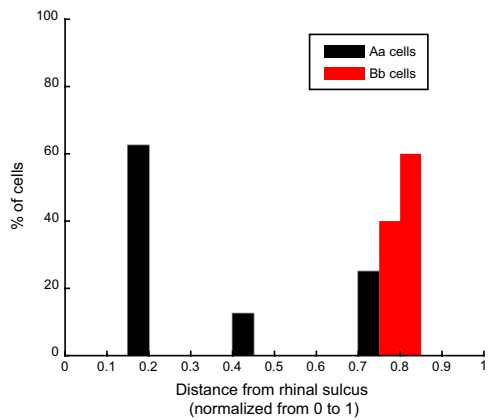
in LEC of WT mice injected with AAV-hSyn-Jaws-GFP into mPFC for inhibition of mPFC terminals in the LEC (Fig. 4 and Extended Data Fig. 17). **(e)** Recording positions in mPFC of WT mice (Fig. 2). Positions were marked with electrolytic lesioning. **(f)** Optic fiber positions in mPFC of WT mice injected with AAV-hSyn-Jaws-GFP into mPFC for inhibition experiments (Fig. 4). *Mice used for recording LEC_{L5/6} cells + mPFC terminal inhibition; **Mice used for recording mPFC cells + LEC_{L5/6} inhibition.



Extended Data Fig. 2 | See next page for caption.

Article

Extended Data Fig. 2 | Verification of opttagging procedure. **(a)** Spike raster plots of a typical opttagged neuron which is seen to follow 1, 2, 5, and 10 Hz pulse trains (5 ms pulse, 10 pulses per train). **(b)** “Opto-PSTH” of 6 example opttagged neurons. Neurons i-v feature optically evoked spikes with low latency and jitter (Bottom right) An excluded opttagged cell (vi), with a long latency of 9.1 ms, suggesting a synaptically tagged cell. **(c)** Latencies of all opttagged neurons plotted against the jitter of first spike after stimulation. Opttagged neurons had a wide variety of latencies (2-8.5 ms), making it difficult to delineate real opttagged cells and potential synaptically tagged cells. **(d)** PCA trajectories, Euclidian distances, and SI plot of LEC_{L5/6} population as in Fig. 1i, excluding opttagged cells with latency greater than 8.5 ms (n = 213 cells). **(e)** PCA trajectories, Euclidian distances, and SI plot of LEC_{L5/6} population as in Fig. 1i, excluding opttagged cells with latency greater than 5 ms (n = 153 cells). These results show a similar Odor-A and -a representation, and similar Odor-B and -b representation at T5. Thus, although the total population analysis may include some synaptically opttagged neurons, it is likely that our conclusion is not affected by their marginal numbers.



Extended Data Fig. 3 | Cue-outcome profile of LEC_{L5/6} neurons along the dorsoventral axis.

Recorded positions along dorsoventral axis of LEC.

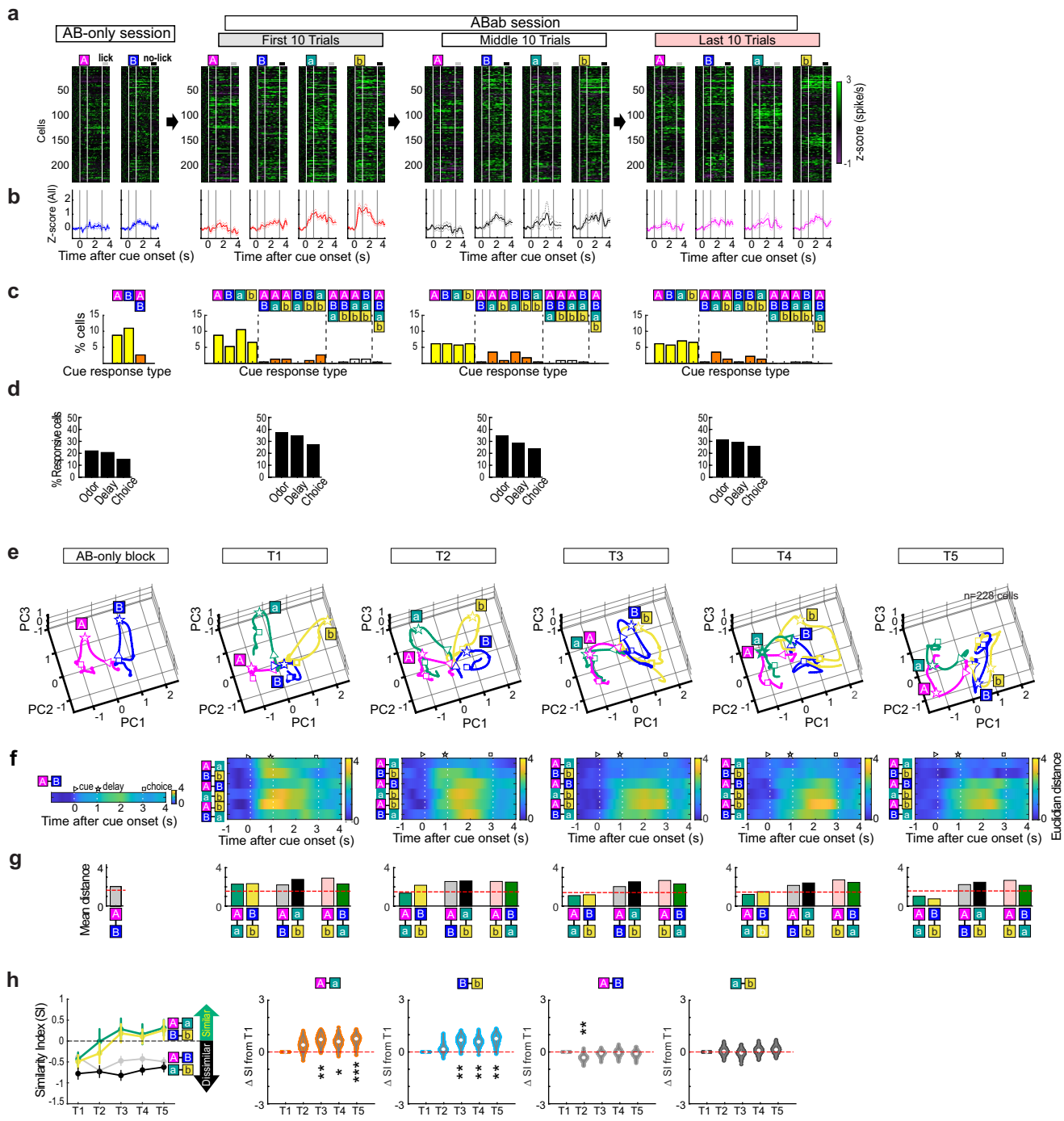
Distances were calculated from rhinal sulcus border to approximate location of

amygdalopiriform transition area and normalized from 0 (dorsal) to 1 (ventral).

The result demonstrated that while Aa cells were observed along the D-V axis,

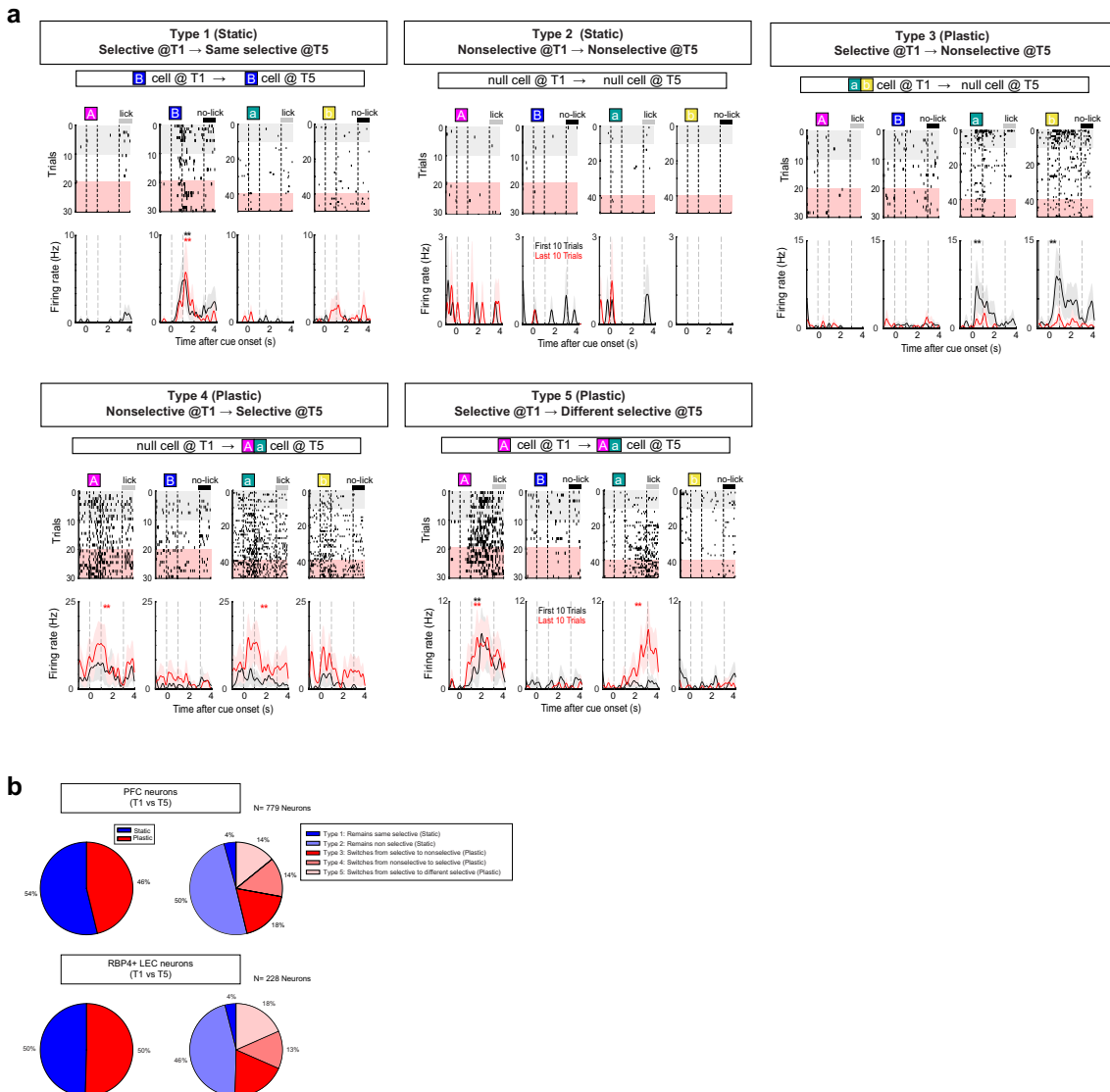
Bb cells were found only in the ventral part of the LEC.

Article



Extended Data Fig. 4 | Spike properties of LEC_{15/6} cells during correct associative learning. (a-d) Spike properties of LEC_{15/6} cells. LEC_{15/6} cells were recorded in a session with Odor-A and Odor-B (AB-only session). After ~20 trials in AB session, associative learning (ABab) session was tested (T1-T5). (a) Spike firing of 228 LEC_{15/6} cells. Mean spike activity was averaged in 50 ms bins and shown in z-score compared with -1–0 s before odor onset. In this panel, cells were sorted using a cluster analysis of firing property in T5. (b) Mean firing rate of 228 LEC_{15/6} cells shown in z-score. (c) Percent responsive cells for each cue combination. Neurons with significant firing during 0.5–3.0 s after odor onset (odor + delay period) were counted (Wilcoxon signed-rank test, $p < 0.05$). (d) Percent responsive cells in periods of 0.5–1.0 s (odor), 2–3 s (delay) and 3–4 s (choice) after odor onset. Neurons with significant firing ($p < 0.05$) during each period were counted (two-sided signed-rank test). (e) Trajectories of neural firing of LEC_{15/6} cell population as in Fig. 1i, but presented throughout

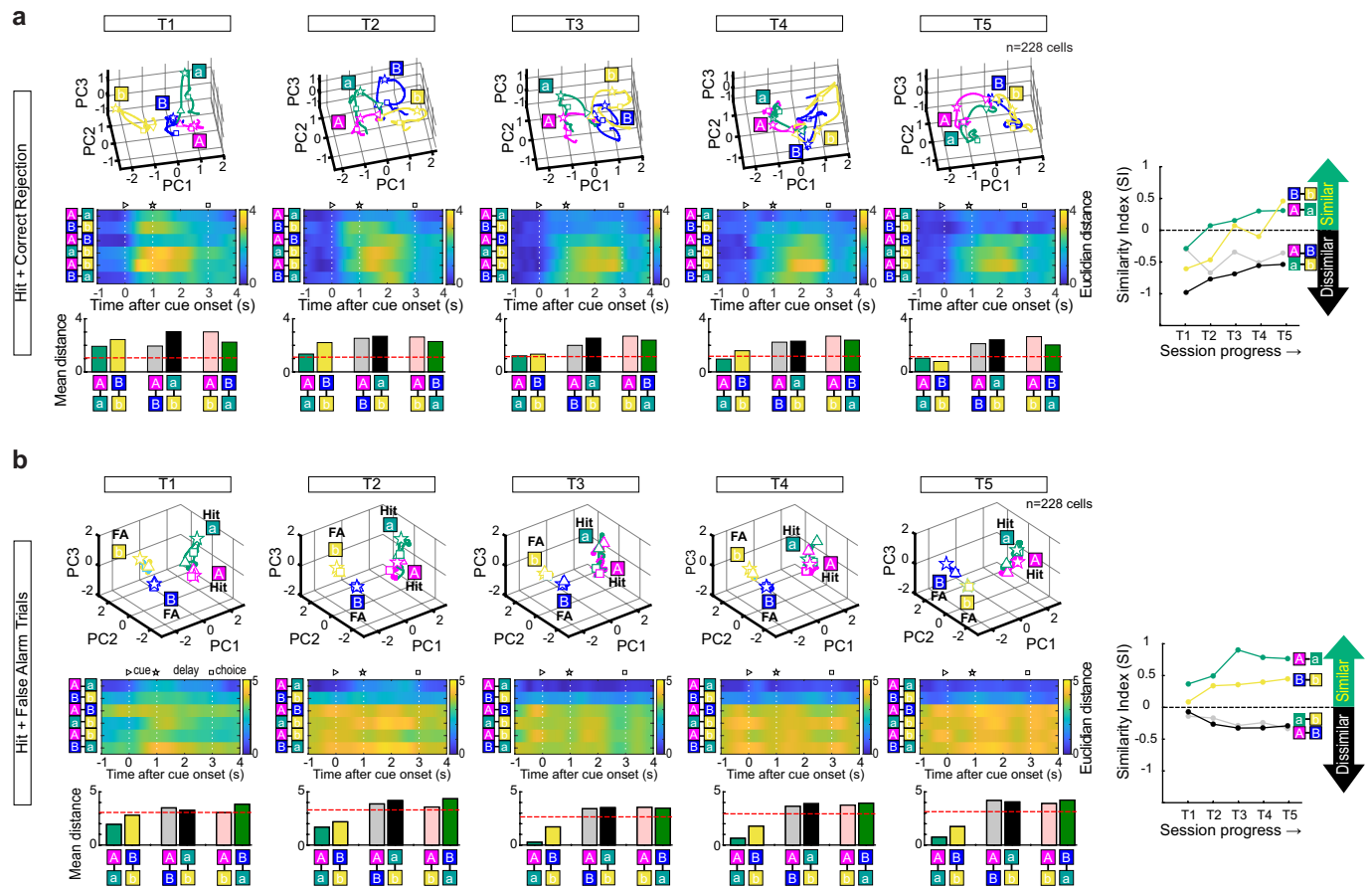
timepoints T1–T5. (f) Euclidian distance between odor trial types. (g) Mean Euclidian distance during 0.5–3.0 s after odor onset (odor + delay period). Ninety-fifth percentile distance obtained from shuffled data denotes significant distance (red line). (h) The change of Similarity Index (SI) during associative learning was compared using the bootstrapping method (see Methods). PCA was performed from a resampled neuronal population, and this procedure was repeated 1000 times to make 1000 bootstraps. SI was calculated for each bootstrap, then SIs in T2–T5 were subtracted by that in T1, to test if there was a significant distribution above or below zero. SI for Odors A-a increased at T3–5 ($p = 0.005, 0.012, 0.0005$ respectively, bootstrapping test), as well as SI for Odors B-b at T3–5 ($p = 0.0023, 0.0021, 0.003$ respectively), confirming increasing similarity of representations between Odor-A and a, and between B-b during leaning. * $p < 0.05$, ** $p < 0.01$, *** $p < 0.001$, two-sided bootstrapping test. Data are presented as mean values +/- SEM.



Extended Data Fig. 5 | Selectivity profile of mPFC and LEC_{LS/6} single neurons during learning. (a) Examples of neurons based on their selectivity profile between T1 vs T5 period. Type 1: Static cells with same selectivity to an odor cue; Type 2: Static cells without selectivity to any cue; Type 3: Plastic cells with selectivity in T1 to an odor cue but no selectivity in T5; Type 4: Plastic cells with no selectivity in T1 but gained selectivity to an odor cue in T5; Type 5: Plastic cells with selectivity to an odor cue in T1 but gained distinct selectivity in T5. Significant selectivity ($p < 0.05$) was assessed using spike response during

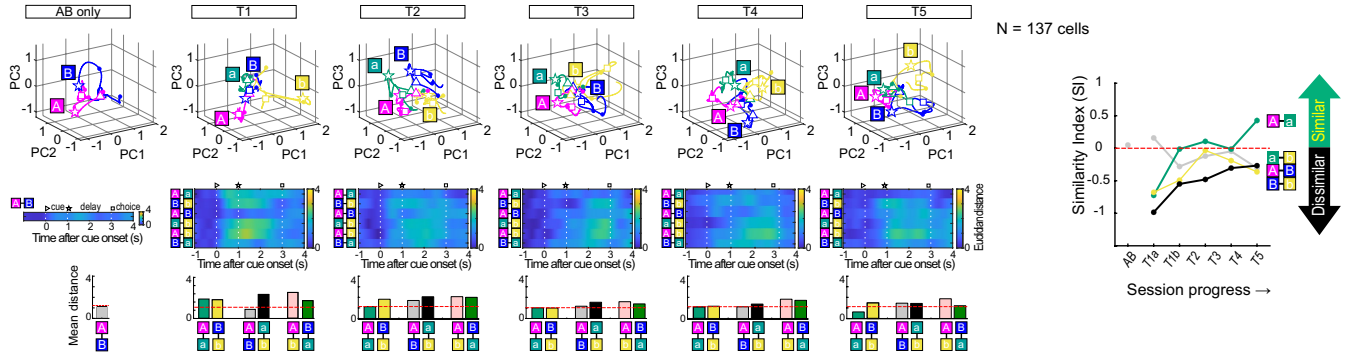
0.5 – 3 s after cue onset, compared to 1 s pre-cue period (two-sided rank sum test). Data are presented as mean values \pm SEM. (b) (Top) Percentage of static (54%) or plastic (46%) mPFC cells. Static cells were further subdivided into type1 (4%) and type 2 (50%). Plastic cells were further subdivided into type3 (18%), type 4 (14%), and type 5 (14%). (Bottom) Percentage of static (50%) or plastic (50%) LEC5/6 cells. Static cells were further subdivided into type1 (4%) and type 2 (46%). Plastic cells were further subdivided into type 3 (19%), type 4 (13%), and type 5 (18%).

Article



Extended Data Fig. 6 | Additional principal component analyses for LEC_{L5/6} cell recordings. (a) Error-exclusion analysis. Trajectories of neural firing of LEC_{L5/6} cell population using only correct (hit) trials for Odors-A and -a and correct rejection (CR) trials for Odors-B and -b. The pattern of A-a vs. B-b dichotomous classification was again observed when the incorrect trials were removed from the PC analysis, excluding the possibility that the representations

in Fig. 1i emerged from the increasing rate of correct trials. (b) Movement analysis. Trajectories of neural firing of LEC_{L5/6} cell population using only lick (hit) trials for Odors-A and -a, and error lick (false alarm, FA) trials for Odors-B and -b. Although all of them are trials in which mice made lick responses, the A-a vs. B-b dichotomous classification similar to Fig. 1i was observed, suggesting that LEC_{L5/6} cells do not simply represent lick-related motor information.

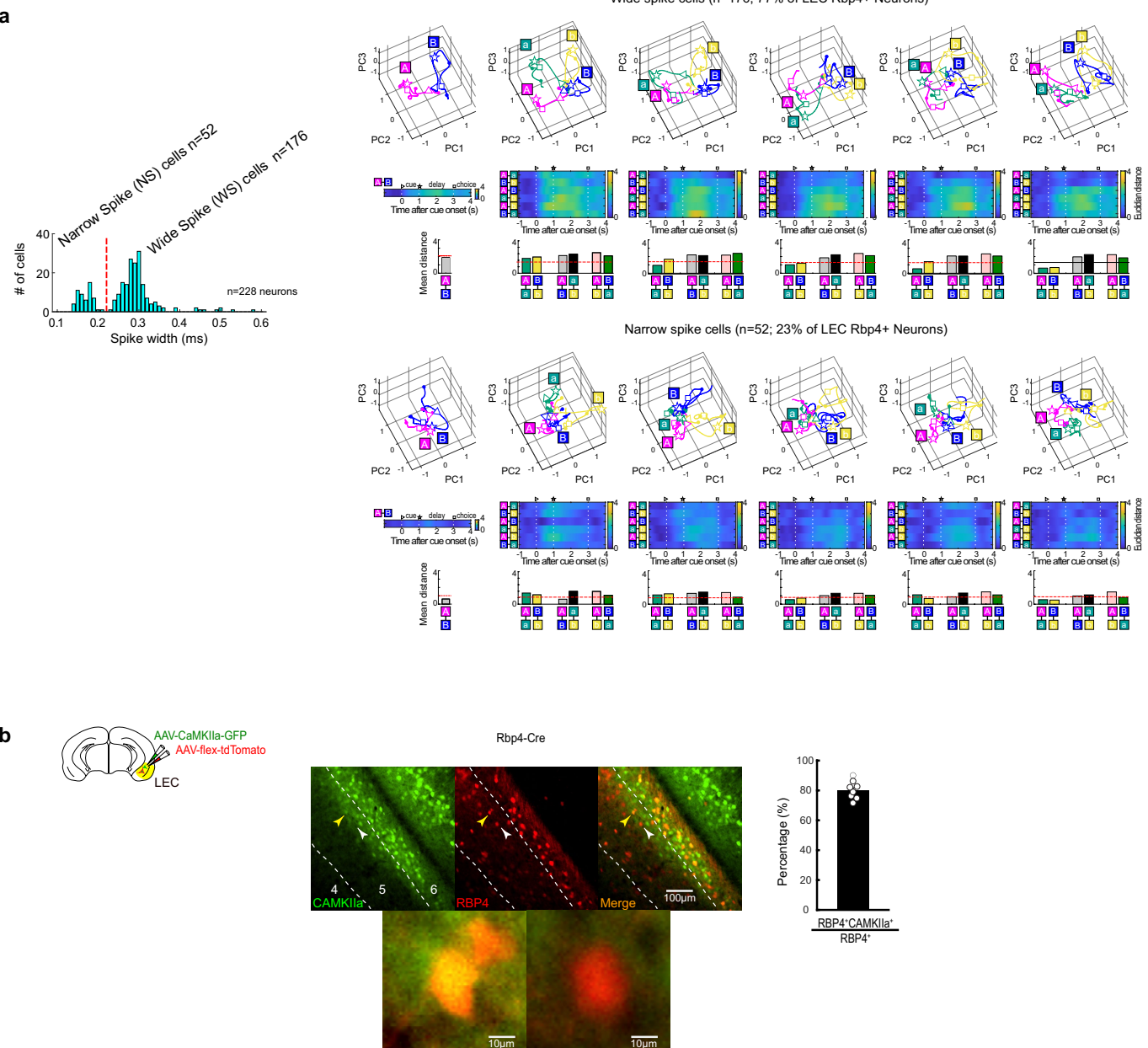


Extended Data Fig. 7 | Effect of individual Aa and Bb cells on population activity

activity. PCA trajectories, Euclidian distances, and SI plot of LEC_{L5/6} population, excluding individual Aa and Bb cells ($n = 137$ cells). The result showed unstable grouping between Odor-A and Odor-a (shown by unstable SI_{A-b} in the SI plot),

and no development of grouping between Odor-B and Odor-b (shown by low SI_{B-b} throughout the session). This result suggests that Aa cells and Bb cells contribute to the generation of outcome rule representation.

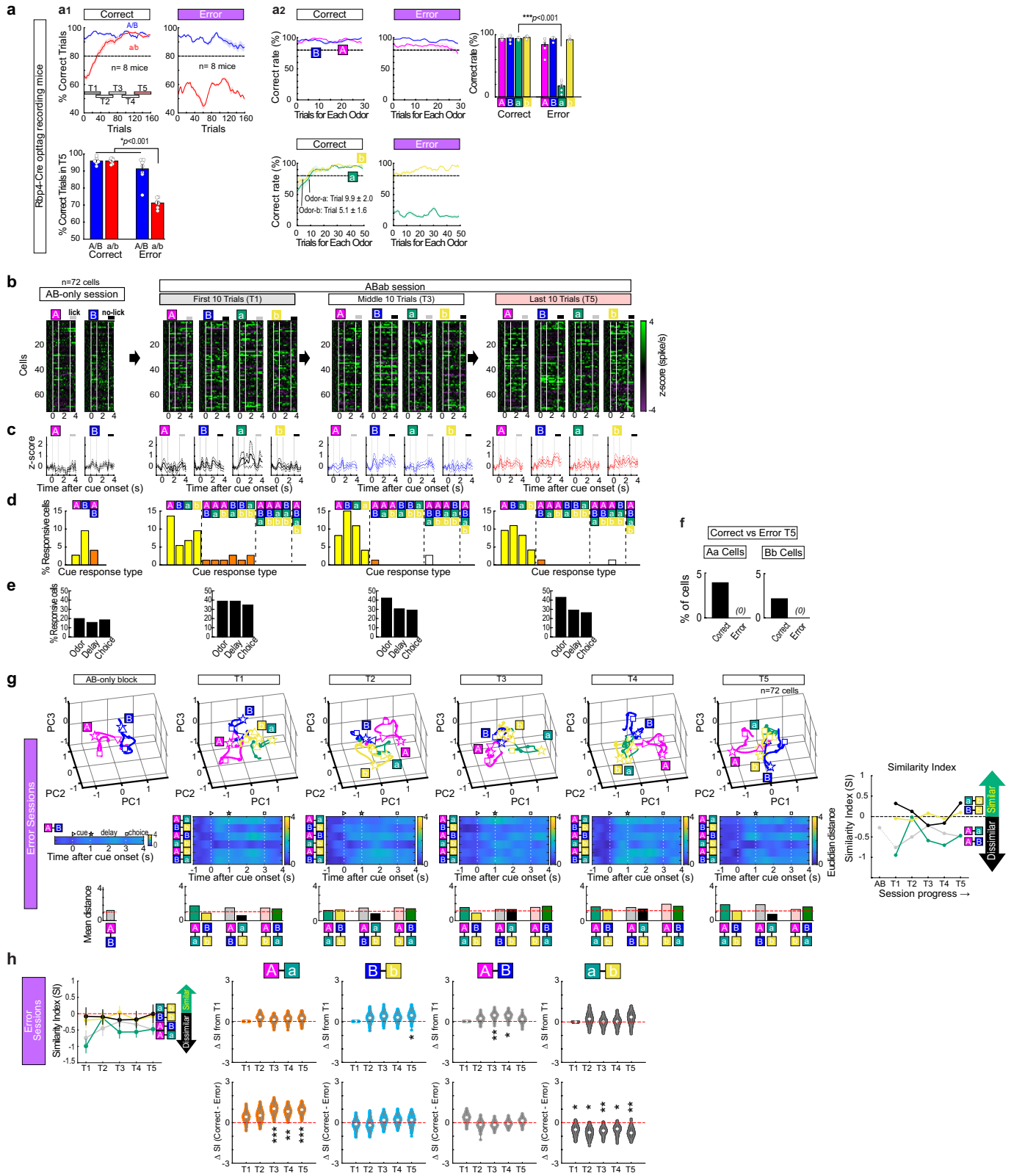
Article



Extended Data Fig. 8 | Characteristics of *Rbp4*⁺ LEC_{1/4} cells.

(a) Electrophysiological features for classifying putative principal neurons. Peak to valley time of spike waveform was used to distinguish putative interneurons from principal neurons in *Rbp4*^{-/-} LEC_{L5/6} cells. (Left) Dashed line (230μs) represents cut off for wide spike (WS) excitatory neurons ($n = 176$; 77%) to narrow spike (NS) interneurons ($n = 52$; 23%) classification (Bartho et al., 2004). (Right) Independent trajectories of neural firing of LEC_{L5/6} WS neurons and NS neurons both demonstrated the grouping of Odors-A and -a and grouping of Odors-B and -b. **(b)** LEC_{L5/6} labeling with excitatory cell marker.

(Left) AAV-flex-tdTomato (red) and AAV-flex-CaMKIIa-GFP (green) were injected into LEC5/6 of *Rbp4-Cre* mice. (Middle) Coronal sections of LEC layer 5/6. CaMKIIa (green) GFP signal reveals excitatory neurons. TdTomato (red) signal reveals *Rbp4*⁺ LEC_{LS/6} cells. Bottom panel demonstrates magnified windows from top panel. Yellow arrow points to example LEC_{LS/6} excitatory cell expressing both CaMKIIa GFP and tdTomato. White arrow points to example LEC_{LS/6} non-excitatory cell expressing only tdTomato. (Right) Percentage of double-positive neurons among tdTomato+ neurons ($80.08 \pm 2.75\%$ from 8 sections obtained from $n = 2$ mice). Data are presented as mean values \pm SEM.

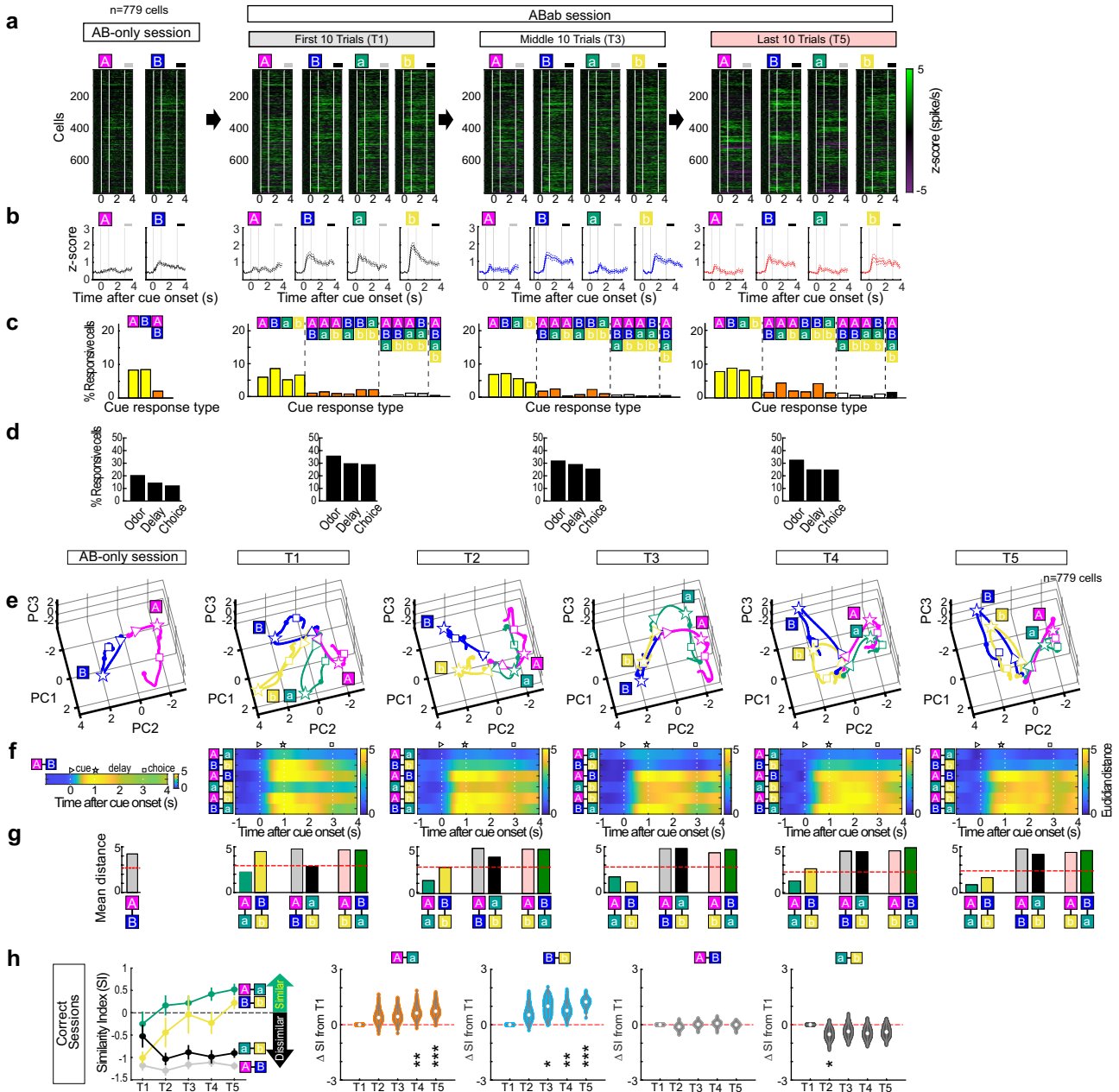


Extended Data Fig. 9 | See next page for caption.

Article

Extended Data Fig. 9 | Spike properties of LEC_{L5/6} cells during spontaneous error sessions. (a) Behavioral performance of LEC *Rbp4-Cre* recording mice in correct sessions (Fig. 1) and error sessions where mice spontaneously could not reach >80% performance criteria. Data are presented as mean values +/- SEM. (a1) Top, learning curves during correct and error sessions. Familiar cue performance (A/B) in blue, novel cue performance (a/b) in red. Bottom, percent correct trials in T5 for correct vs. error sessions ($p = 8.8e-8$, two-way ANOVA; A/B correct vs. a/b error, * $p = 3.8e-9$ or less, post-hoc Tukey test; $n = 8$ mice). (a2) (Left) Percentage of correct trials plotted in each odor trial type. (Right) Performance of mice in the last 10 trials ($p = 4.8e-28$, two-way ANOVA; *** $p = 6e-8$ between Odor-a correct vs. odor-a error, post-hoc Tukey test; $n = 8$ mice). (b-e) Same as in Extended Data Fig. 4a-d, but for error sessions ($n = 72$ cells). (f) Proportion of Aa cells (left) and Bb cells (right) in correct vs. error sessions.

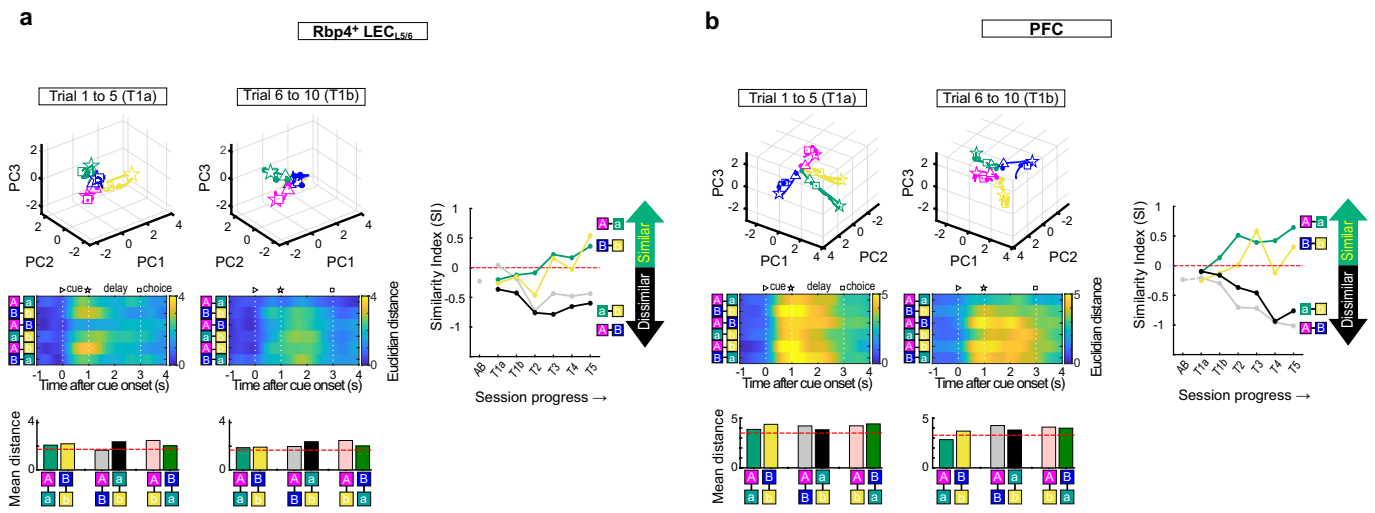
Both response types were missing in error sessions. (g) Same as in Extended Data Fig. 4e-g, but for error sessions. SI plot shows that SI_{Aa} did not increase to positive, indicating Odor-a was not classified together with Odor-A. (h) Bootstrapping analysis. (Top) Same plot as in Extended Data Fig. 4h, but for error sessions. LEC_{L5/6} cells did not develop similar representations between Odors-A and -a, and between Odors-B and -b observed in correct sessions. (Bottom) Direct comparison between correct and error sessions confirmed the disappearance of similar representations between Odors-A and -a at T3-T5 of error sessions ($p = 0.27, 0.14, 0.13$ respectively). The comparison also indicates more similar representations between Odors-a and -b throughout error sessions T1-T5 ($p = 0.043, 0.013, 0.0056, 0.026, 0.0054$ respectively). * $p < 0.05$, ** $p < 0.01$, *** $p < 0.001$, two-sided bootstrapping test. Data are presented as mean values +/- SEM.



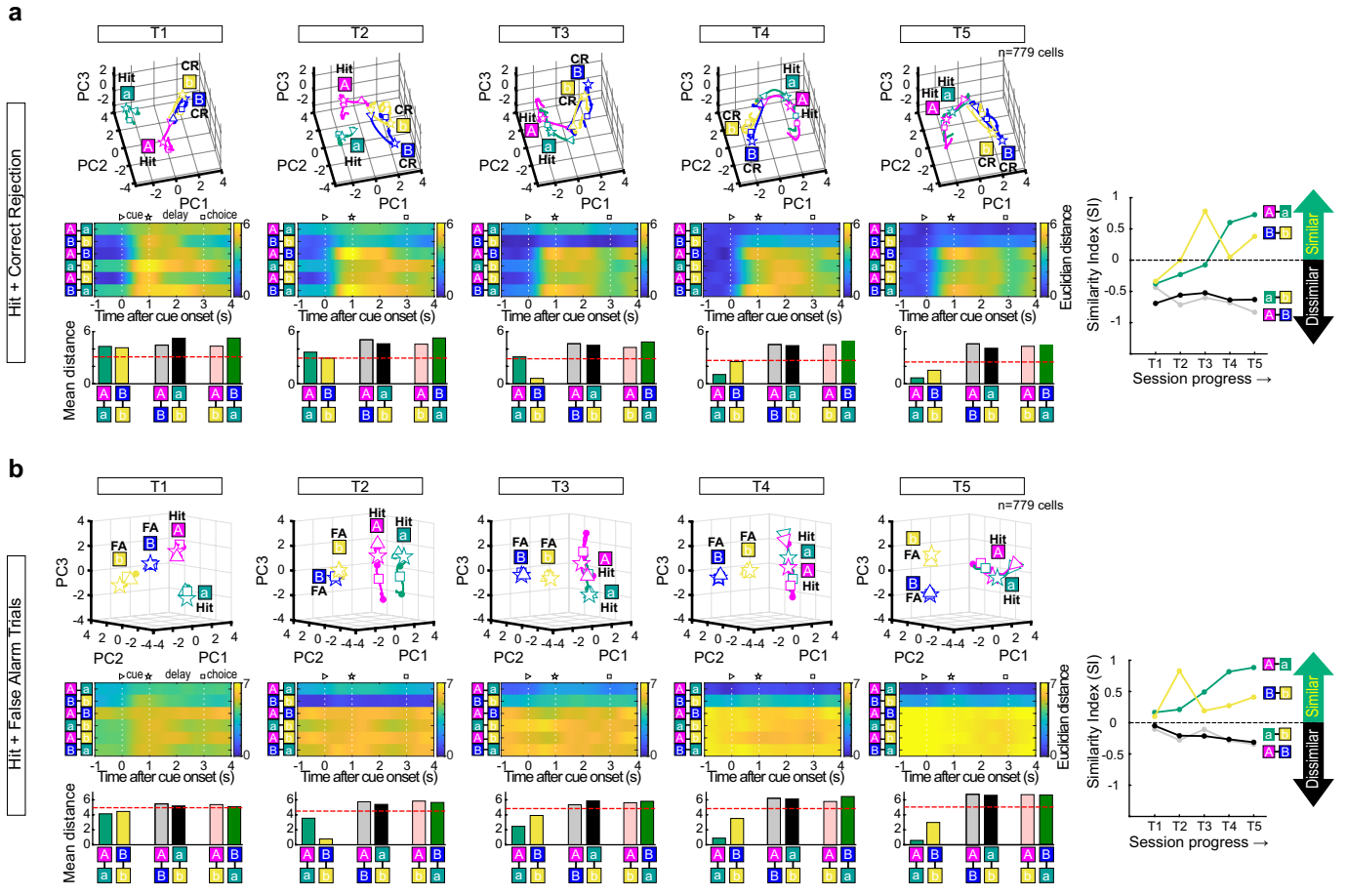
Extended Data Fig. 10 | Spike properties of mPFC cells during correct associative learning sessions. (a) Spike firing of 779 mPFC cells. Mean spike activity was averaged in 50 ms bins and shown in z-score compared with $-1 - 0$ s before odor onset. In this panel, cells were sorted using a cluster analysis of firing property in T5. (b) Mean firing rate of 779 mPFC cells shown in z-score. (c) Percent responsive cells in correct T5 (top) and error T5 (bottom). Neurons with significant firing ($p < 0.05$) during 0.5–3.0 s after odor onset (odor + delay period) were counted (two-sided signed-rank test). (d) Percent responsive cells in periods of 0.5–1.0 s (odor), 2–3 s (delay) and 3–4 s (choice) after odor onset. Neurons with significant firing ($p < 0.05$) during each period were counted (two-sided signed-rank test). (e) Trajectories of neural firing of mPFC cell population as shown in Fig. 2h, but for timepoints T1 – T5. (f) Euclidian distance

between odor trial types. (g) Mean Euclidian distance during 0.5–3.0 s after odor onset (odor + delay period) for timepoints T1 – T5 of correct sessions. Ninety-fifth percentile distance obtained from shuffled data denotes significant distance (red line). (h) Bootstrapping analysis for Fig. 2j. SI for Odors A-a and B-b showed significant increases in T5 compared to T1 ($p = 0.0039$ and $p = 1.7e-8$, respectively, bootstrapping test), while SI for Odors A-B and a-b showed significant decreases ($p = 3.1e-5$ and $p = 0.029$, respectively), confirming increasing similarity between odors of the same outcome, and decreasing similarity between odors of the different outcome. * $p < 0.05$, ** $p < 0.01$, *** $p < 0.001$, two-sided test, $n = 1000$ bootstraps each. Data are presented as mean values \pm SEM.

Article



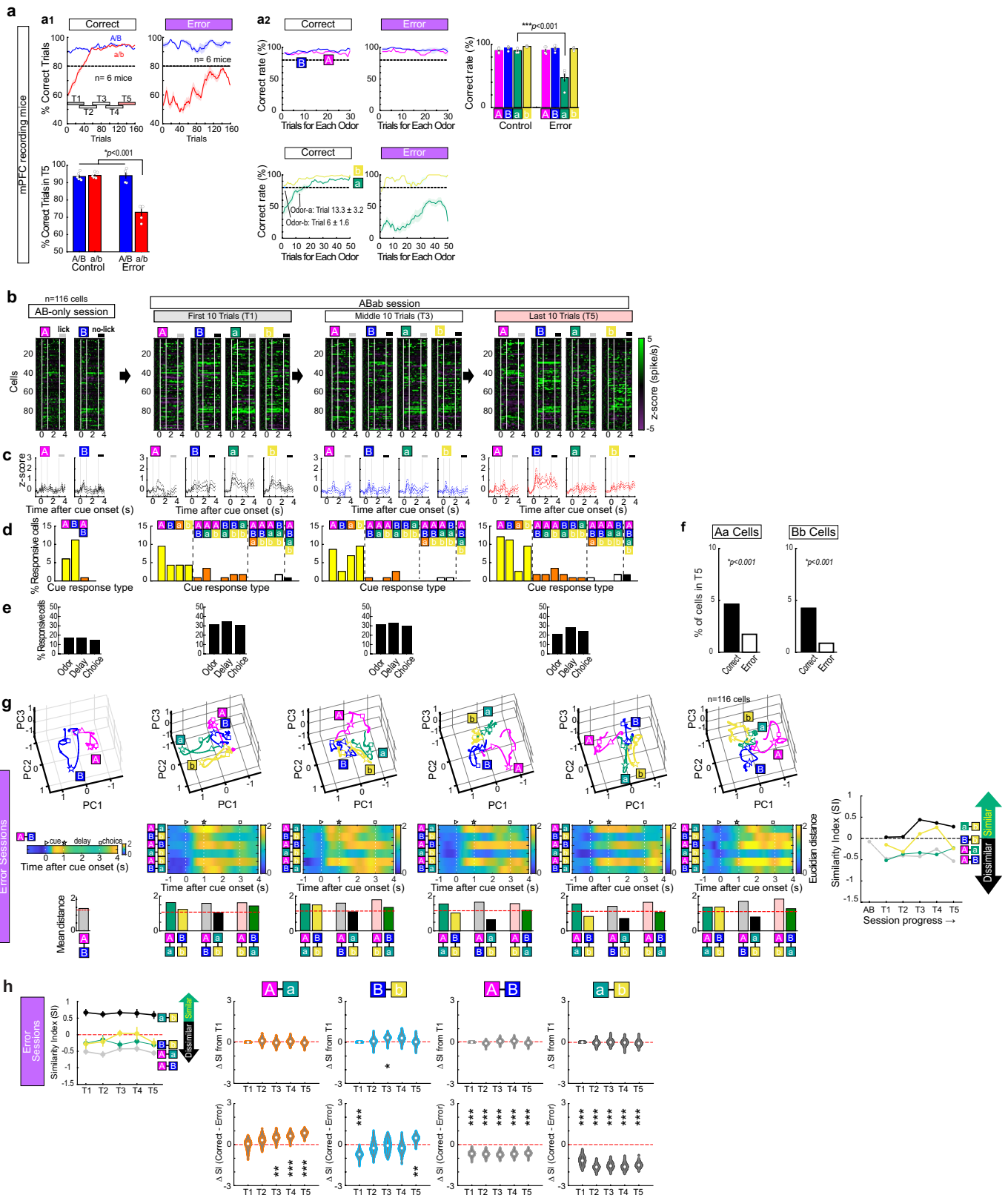
Extended Data Fig. 11 | Early emergence of grouping of Odor-A and Odor-a rewarded cues. (a) Trajectories of neural firing of LEC_{L5/6} cell population as in Fig. 1i, but presented throughout timepoints T1a (first five trials of T1) and T1b (second five trials of T1). (b) Trajectories of neural firing of mPFC cell population as above.



Extended Data Fig. 12 | Additional principal component analyses for mPFC cell recordings. (a) Error-exclusion analysis. Trajectories of neural firing of mPFC cell population using only correct (hit) trials for Odors-A and -a, and correct rejection (CR) trials for Odors-B and -b. The pattern of A-vs. B-b dichotomous classification was again observed when the incorrect trials were removed from the PC analysis, excluding the possibility that the representations

in Fig. 2h emerged from the increasing rate of correct trials. (b) Movement analysis. Trajectories of neural firing of mPFC cell population using only lick (hit) trials for Odors-A and -a and error lick (false alarm, FA) trials for Odors-B and -b. Although all of them are trials in which mice made lick responses, the A-a vs. B-b dichotomous classification similar to Fig. 2h was observed, suggesting that mPFC cells do not simply represent lick-related motor information.

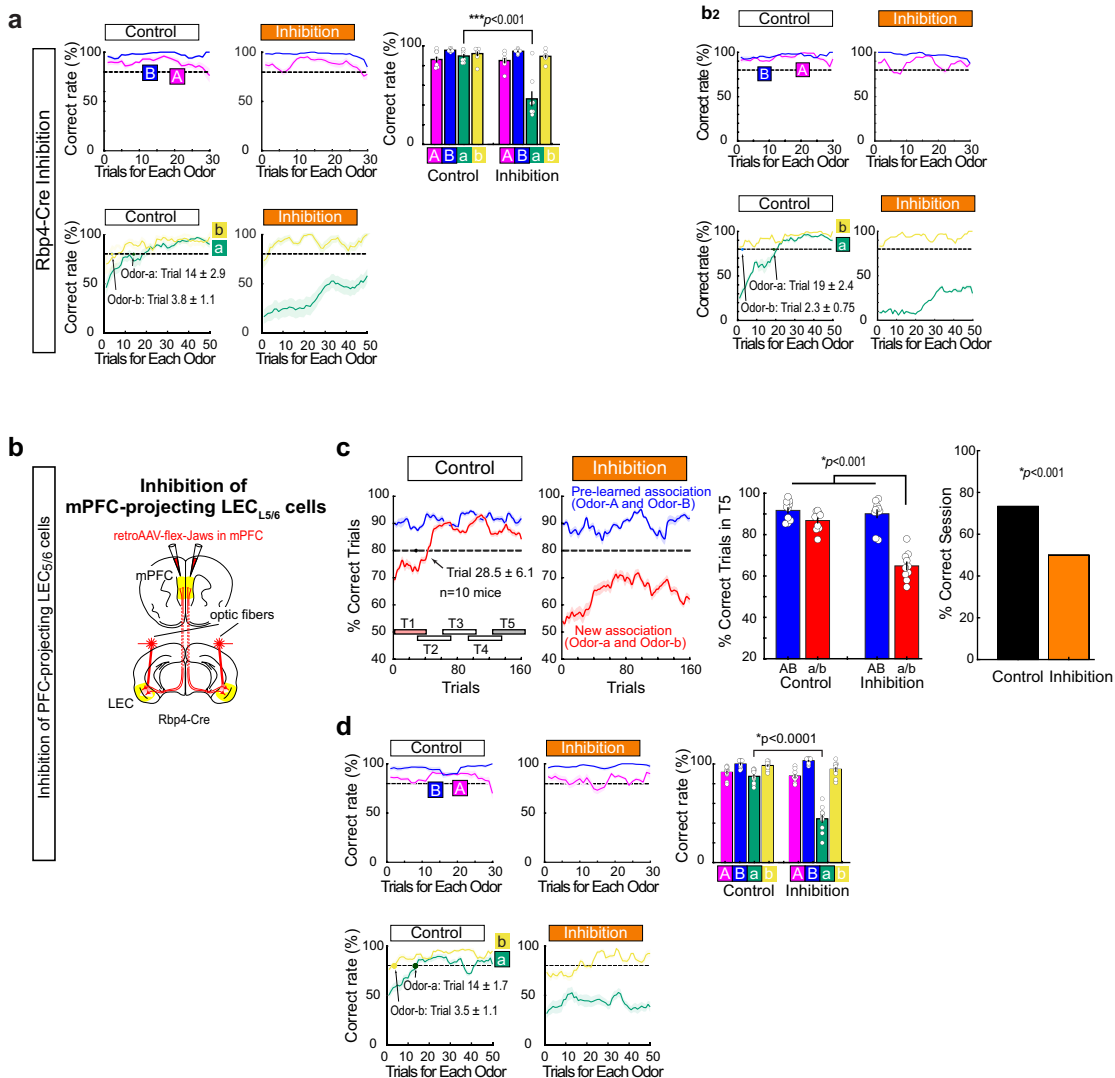
Article



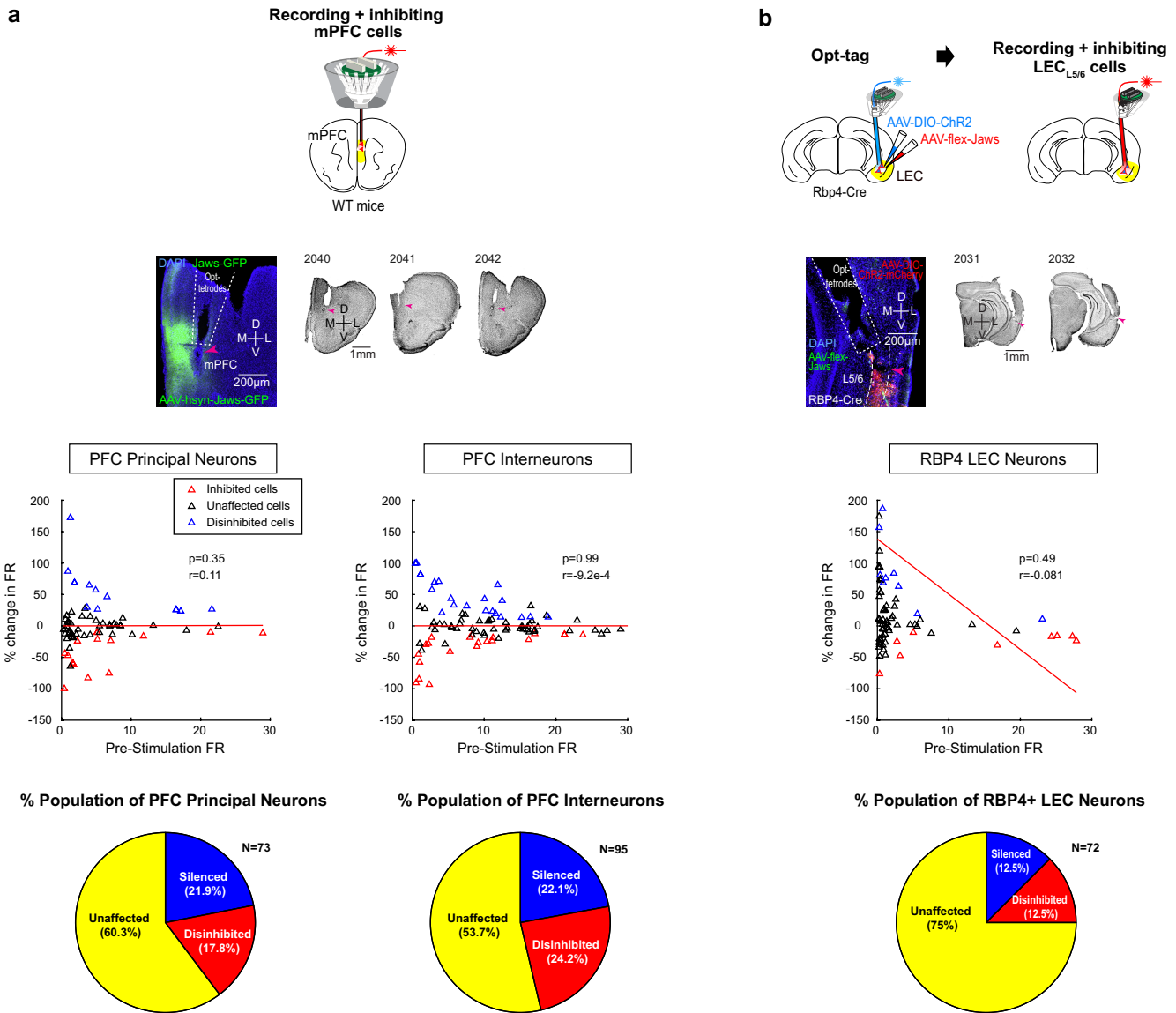
Extended Data Fig. 13 | See next page for caption.

Extended Data Fig. 13 | Spike properties of mPFC cells during spontaneous error sessions. (a) Behavioral performance of mPFC recording mice in correct sessions (Fig. 2) and error sessions where mice spontaneously could not reach >80% performance criteria. Data are presented as mean values +/- SEM. (a1) Behavioral performance of mPFC recording mice in correct vs. error sessions. Top, learning curves during correct and error sessions. Familiar cue performance (A/B) in blue, novel cue performance (a/b) in red. Bottom, percentage of correct trials in T5 for correct vs. error sessions ($p = 2.4e-7$, ANOVA; $p = 1.9e-8$ or less, post-hoc Tukey test; $n = 6$ mice). (a2) mPFC recording mice data plotted for percent correct trials in each odor trial type as a function of trial number for each odor type. (Right) Performance of mice in the last 10 trials ($p = 1.99e-11$, ANOVA; *** $p = 6e-8$ between Odor-a correct vs. odor-a error, post-hoc Tukey test; $n = 6$ mice). (b-e) Same as in Extended Data Fig. 10a-d, but for error sessions ($n = 116$ cells). (f) Proportion of mPFC Aa cells (left) and Bb cells (right) in correct vs. error sessions. Aa: $p = 1.8e-7$, Bb: $p = 2.2e-13$, two-sided

binomial test. (g) Same as in Extended Data Fig. 10e-g, but for error sessions. (h) Bootstrapping analysis. (Top) Same plot as in Extended Data Fig. 10h, but for error sessions. During the error sessions, mPFC cells did not develop similar representations between Odors-A and -a (T2-T5: $p = 0.24, 0.39, 0.36, 0.36$, respectively) and between Odors-B and -b (T2-T5: $p = 0.36, 0.034, 0.089, 0.43$, respectively) observed in correct sessions. (Bottom) Direct comparison between correct and error sessions confirmed the disappearance of similar representations between Odors-A and -a (T3-T5: $p = 0.006, 0.0005, 6.3e-8$, respectively), and similar representations between Odors-B and -b (T5, $p = 0.0002$). The comparison also indicates more similar representations between Odors-A and -B (T1-T5: $p = 3e-6, 1.8e-6, 6.2e-8, 4e-7, 1.2e-7$, respectively), and between Odors-a and -b throughout the error sessions (T1-T5: $p = 7e-6, 1e-16, 3e-15, 1e-16, 1e-16$, respectively). * $p < 0.05$, ** $p < 0.01$, *** $p < 0.001$, bootstrapping test, $n = 1000$ bootstraps each. Data are presented as mean values +/- SEM.



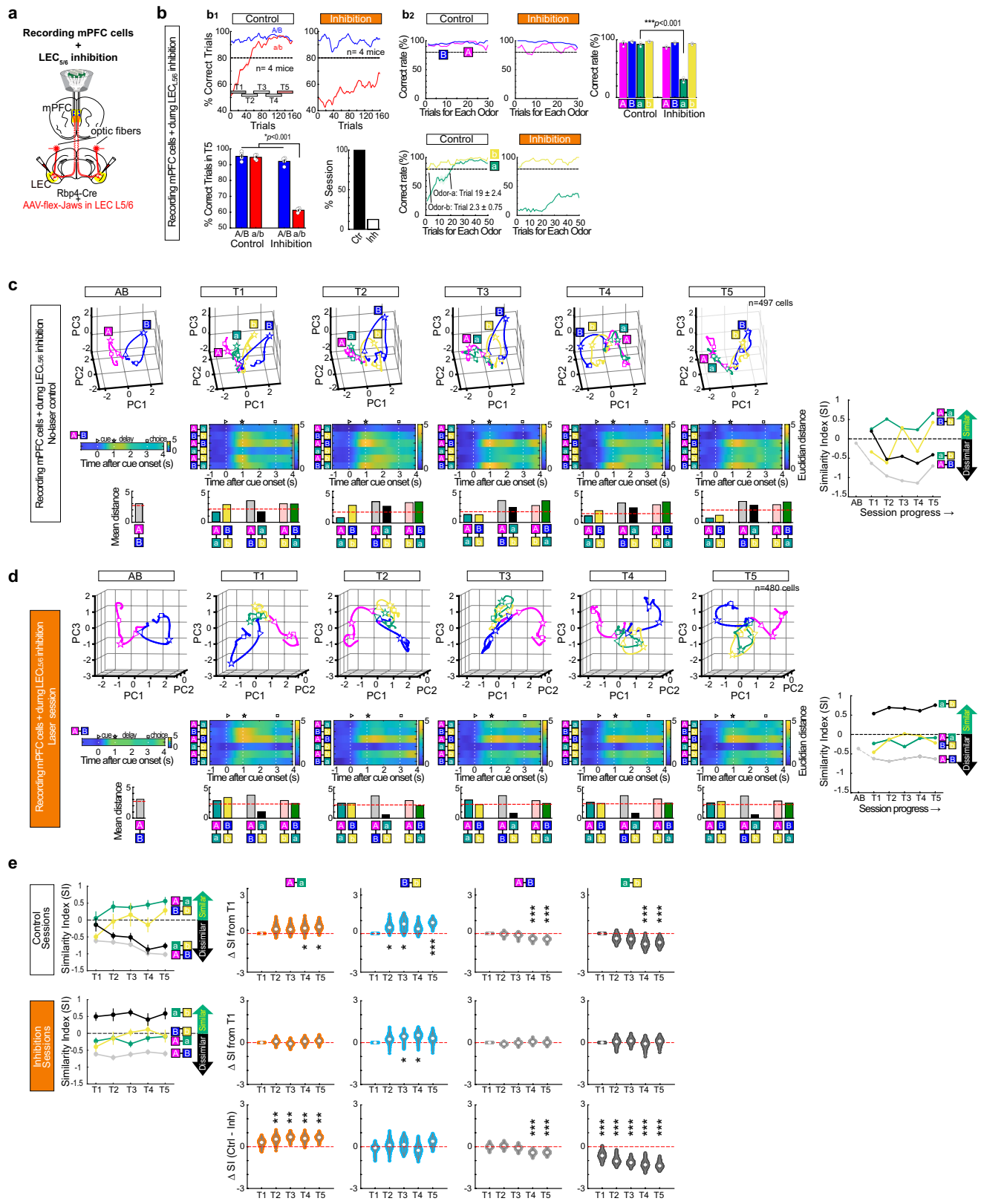
Extended Data Fig. 14 | Behavioral performance in LEC_{L5/6} inhibition experiments. (a) Behavioral performance of LEC *Rbp4-Cre* mice in Fig. 3a,b, but plotted for each odor trial type. Learning curves during control (left) and LEC_{L5/6} inhibition (middle) sessions. (Right) Performance of mice in the last 10 trials ($p = 3.8e-13$, two-way ANOVA; $p = 6e-8$ between Odor-a in control vs. Odor-a inhibition sessions, post-hoc Tukey test; $n = 10$ mice). Data are presented as mean values +/- SEM. (b-d) mPFC-projecting LEC_{L5/6} cell inhibition experiments. Data are presented as mean values +/- SEM. (c) (Left) Learning curves during control and inhibition sessions. (Middle) Percent correct trials in T5 for control vs. inhibition sessions ($p = 3.4e-6$, two-way ANOVA; A/B control vs. a/b inhibition, $p = 3.8e-9$; a/b correct vs. a/b error, $p = 7.2e-9$; A/B error vs. a/b error, $p = 3.9e-9$, post-hoc Tukey test; $n = 10$ mice). (Right) Proportion of correct sessions between control and inhibition conditions ($p = 0.0064$, two-sided binomial test; $n = 30$ control and 30 inhibition sessions). (d) Percent correct trials in each odor trial type as a function of trial number for each odor type. (Right) Performance of mice in the last 10 trials ($p = 1.5e-16$, two-way ANOVA; $p = 6e-8$ for Odor-a in correct sessions vs. odor-a in error sessions, post-hoc Tukey test; $n = 10$ mice).



Extended Data Fig. 15 | Modulation of neuronal activity with Jaws inhibition. (a) (Top) Recording of mPFC cells during inhibition. Jaws were expressed in mPFC cells using synapsin promoter driven AAVs. (Middle) Correlation between change in firing rate and pre-stimulation firing rate divided into principal neurons and interneurons based on their spike waveform peak-to-trough width threshold of 230 μs. Each dot represents a single cell. Cells were classified as inhibited, unaffected, or disinhibited using two-sided rank sum test ($p < 0.05$ threshold) between pre-stimulation firing rate and firing rate during inhibition. (Bottom) Percentage of inhibited (21.9%), unaffected (60.3%), or disinhibited

(17.8%) mPFC cells during inhibition. (b) (Top) Opt-tag recording of LEC_{L5/6} cells during inhibition. ChR2 and Jaws were expressed in LEC_{L5/6} of *Rbp4-Cre* mice. (Middle) Correlation between change in firing rate and pre-stimulation firing rate. Each dot represents a single cell. Cells were classified as inhibited, unaffected, or disinhibited using two-sided rank sum test ($p < 0.05$ threshold) between pre-stimulation firing rate and firing rate during inhibition. (Bottom) Percentage of inhibited (12.5%), unaffected (75%), or disinhibited (12.5%) LEC_{L5/6} cells during inhibition.

Article



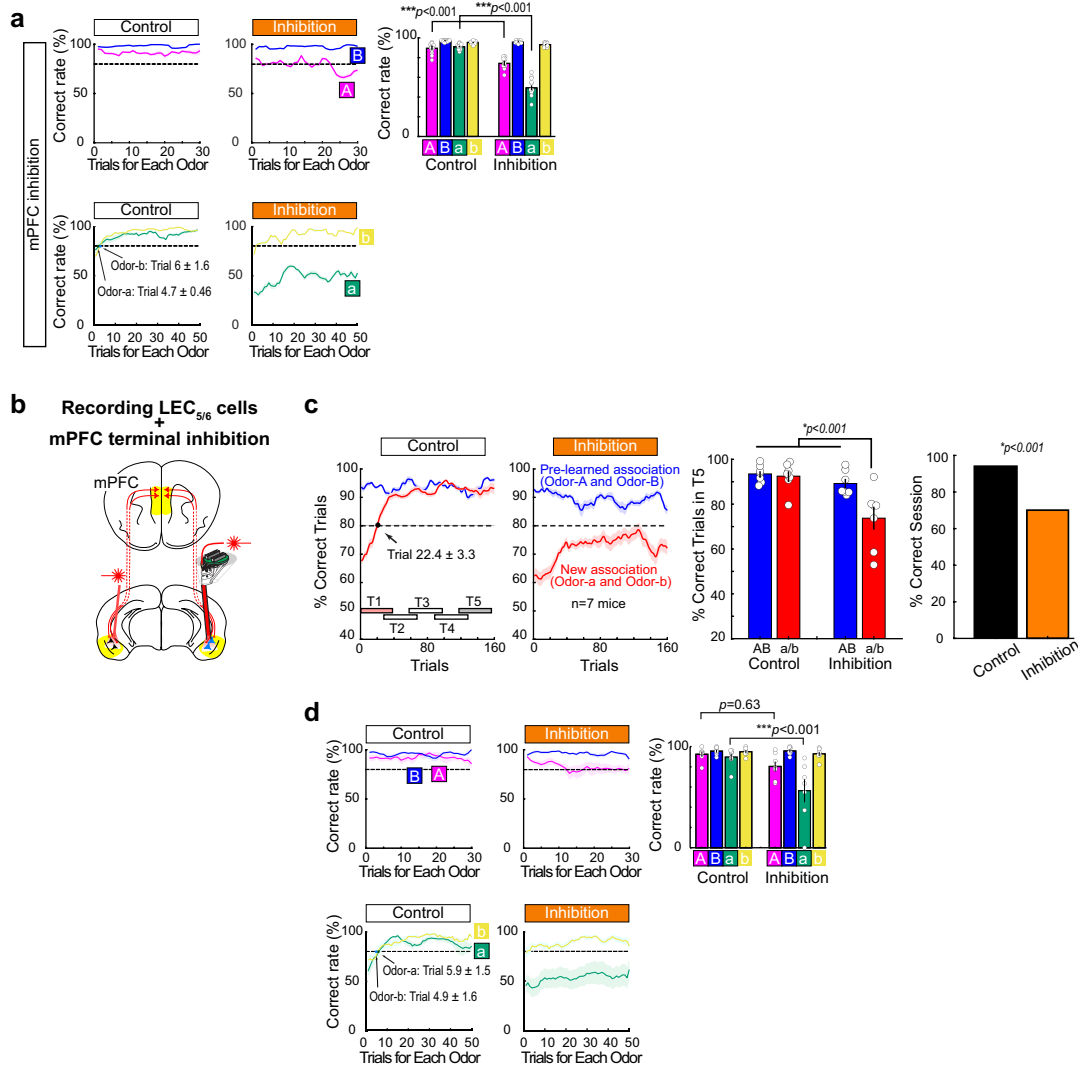
Extended Data Fig. 16 | See next page for caption.

Extended Data Fig. 16 | Detailed analyses from recording of mPFC cells with LEC_{L5/6} inhibition.

(a-b) Behavioral performance only from $n = 4$ mice used in mPFC cell recording with simultaneous inhibition of LEC_{L5/6} cells. **(b1)** (Top) Learning curves during control and inhibition sessions. (Bottom left) Percentage of correct trials in T5 for control vs. inhibition sessions ($p = 7.5e-9$, two-way ANOVA; $p = 5.6e-9$ or less, post-hoc Tukey test; $n = 4$ mice). (Bottom right) Proportion of correct sessions between control and inhibition conditions ($p = 1.6e-10$, two-sided binomial test; $n = 24$ control and 24 inhibition sessions). Data are presented as mean values +/- SEM. **(b2)** Percent correct trials in each odor trial type as a function of trial number for each odor type. (Right) Performance of mice in the last 10 trials ($p = 2.8e-18$, two-way ANOVA; $p = 6e-6$ between Odor-a in correct sessions vs. Odor-a in error sessions, post-hoc Tukey test; $n = 4$ mice). Data are presented as mean values +/- SEM. **(c)** (Top) Trajectories of neural firing of $n = 497$ mPFC cell population in no-laser control sessions. (Middle) Euclidian distance between odor trial types. (Bottom) Mean Euclidian distance during 0.5-3.0 s after odor onset (odor + delay period) for

timepoints T1 – T5 of correct sessions. Ninety-fifth percentile distance obtained from shuffled data denotes significant distance (red line). (Right) Similarity index. **(d)** Same as (c), but for inhibition sessions (laser on). **(e)** Bootstrapping analysis. (Top) In control sessions, SI between Odors A-a and between Odors B-b showed significant increase from T1 to T5 ($p = 0.014$, $p = 2.6e-6$, respectively). SI for Odors A-B and a-b showed significant decrease from T1 to T5 ($p = 5.4e-6$, $p = 0.0027$, respectively, bootstrapping test). (Middle) In inhibition sessions, SI for all odor pairs did not show significant differences from T1 to T5 (Aa: $p = 0.15$, Bb: $p = 0.08$, AB: $p = 0.45$, ab: $p = 0.34$), confirming the impairment of outcome classification. (Bottom) Direct comparison between control and inhibition sessions confirmed the disappearance of similar representations between Odors-A and -a (T5: $p = 7e-6$). The comparison also indicates disappearance of separate representations between Odors-A and -B and between Odors-a and -b in inhibition sessions ($p = 2e-4$, $8e-13$, respectively). $n = 1000$ bootstraps; * $p < 0.05$, ** $p < 0.01$, *** $p < 0.001$, bootstrapping test. Data are presented as mean values +/- SEM.

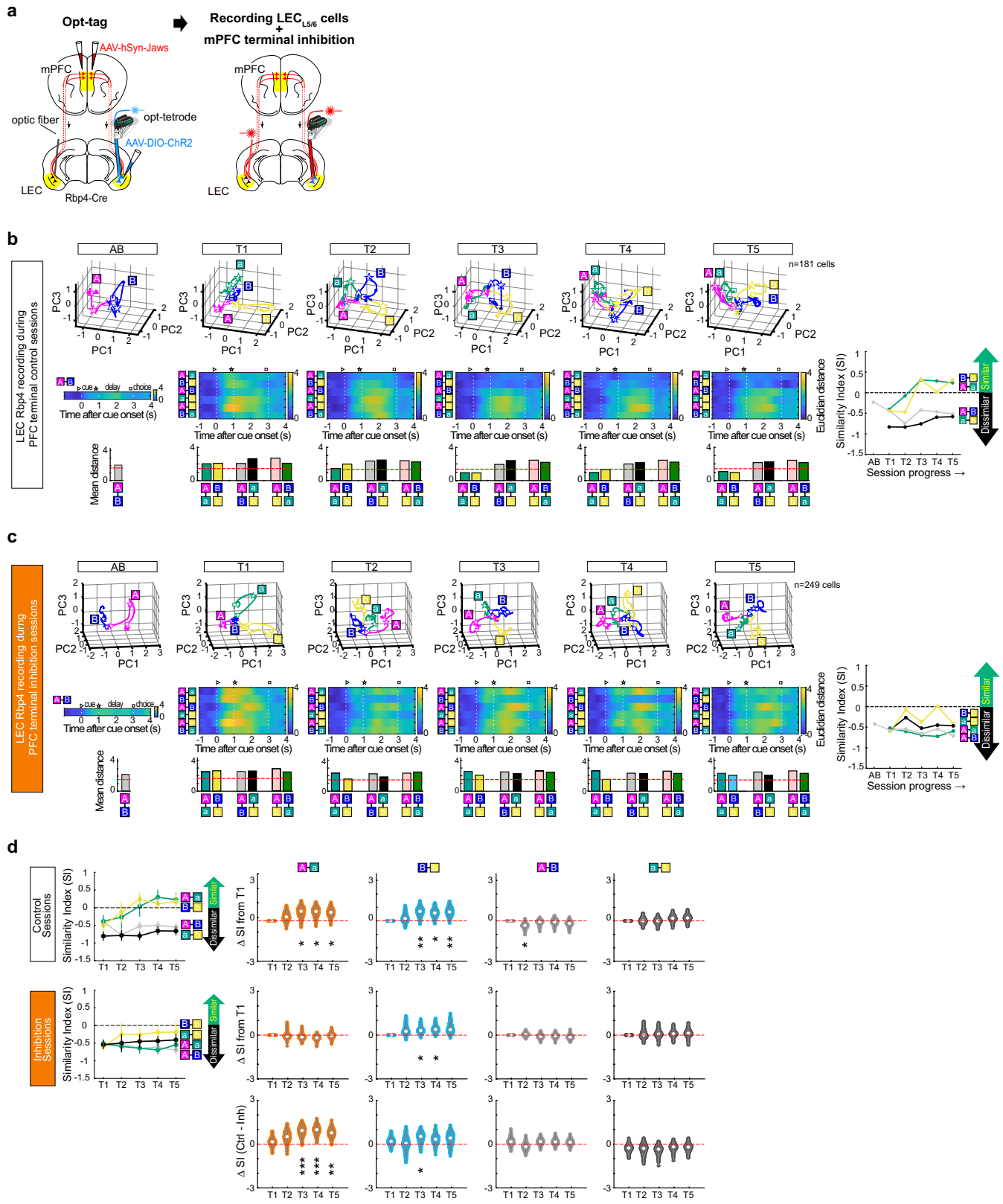
Article



Extended Data Fig. 17 | Behavioral performance for mPFC inhibitions.

(a) Behavioral performance during mPFC inhibition in Fig. 4a,b, but plotted for each odor trial type. Learning curves during control (left) and mPFC inhibition (middle) sessions. (Right) Performance of mice in the last 10 trials ($p = 1e-32$, two-way ANOVA; $p = 6e-8$ between Odor-A in control sessions vs. Odor-A in inhibition sessions; $p = 6e-8$ between Odor-a in control sessions vs. Odor-a in inhibition sessions, post-hoc Tukey test; $n = 13$ mice). Data are presented as mean values +/- SEM. (b-d) Behavior performance during mPFC terminal inhibition. Data are presented as mean values +/- SEM. (c) (Left) Learning curves during control and inhibition sessions. (Middle) Percent correct trials in T5 for

control vs. inhibition sessions ($p = 0.029$, two-way ANOVA; $p = 0.0088$ or less, post-hoc Tukey test; $n = 7$ mice). (Right) Proportion of correct sessions between control and inhibition conditions ($p = 0.0001$, two-way binomial test; $n = 31$ control and 21 inhibition sessions). (d) Percent correct trials in each odor trial type as a function of trial number for each odor type. (Right) Performance of mice in the last 10 trials ($p = 0.0037$, two-way ANOVA; $p = 0.0003$ between Odor-a in correct sessions vs. Odor-a in error sessions, post-hoc Tukey test; $n = 7$ mice). Although not significant, we observed a trend of decrease in the performance for Odor-A during inhibition ($p = 0.63$, Odor-A in correct sessions vs. Odor-A in error sessions, post-hoc Tukey test).

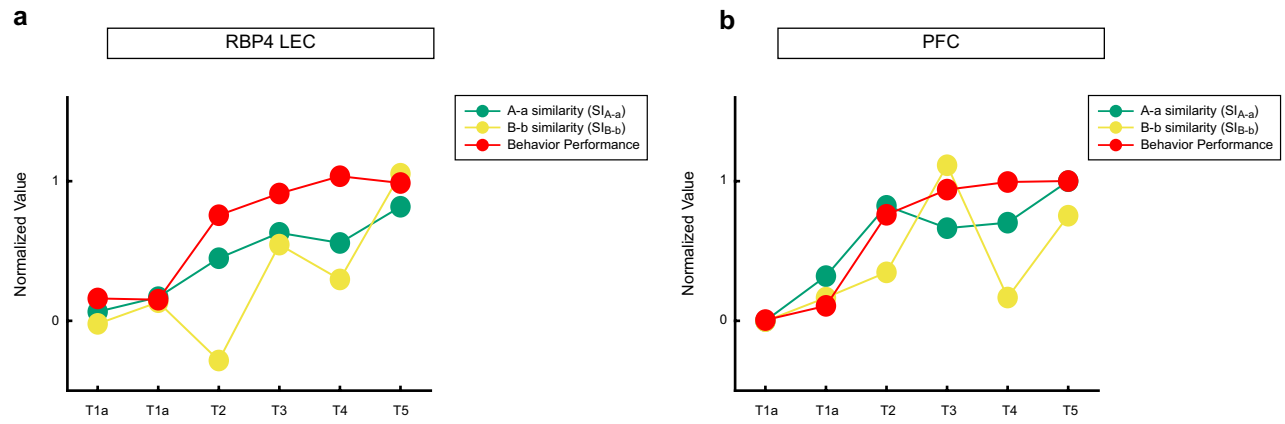


Extended Data Fig. 18 | See next page for caption.

Article

Extended Data Fig. 18 | Detailed analyses from recording of LEC_{L5/6} cells with mPFC terminal inhibition. (a) Opt-tag recording of LEC_{L5/6} cells with simultaneous inhibition of mPFC inputs in LEC. (b) (Top) Trajectories of neural firing of n = 181 LEC_{L5/6} cell population in no-laser control sessions. (Middle) Euclidian distance between odor trial types. (Bottom) Mean Euclidian distance during 0.5–3.0 s after odor onset (odor + delay period) for timepoints T1 – T5 of correct sessions. Ninety-fifth percentile distance obtained from shuffled data denotes significant distance (red line). (Right) Similarity index. (c) Same as (b), but for n = 249 LEC_{L5/6} cell population during mPFC terminal inhibition sessions (laser on). (d) Bootstrapping analysis. (Top) In control sessions, SI between

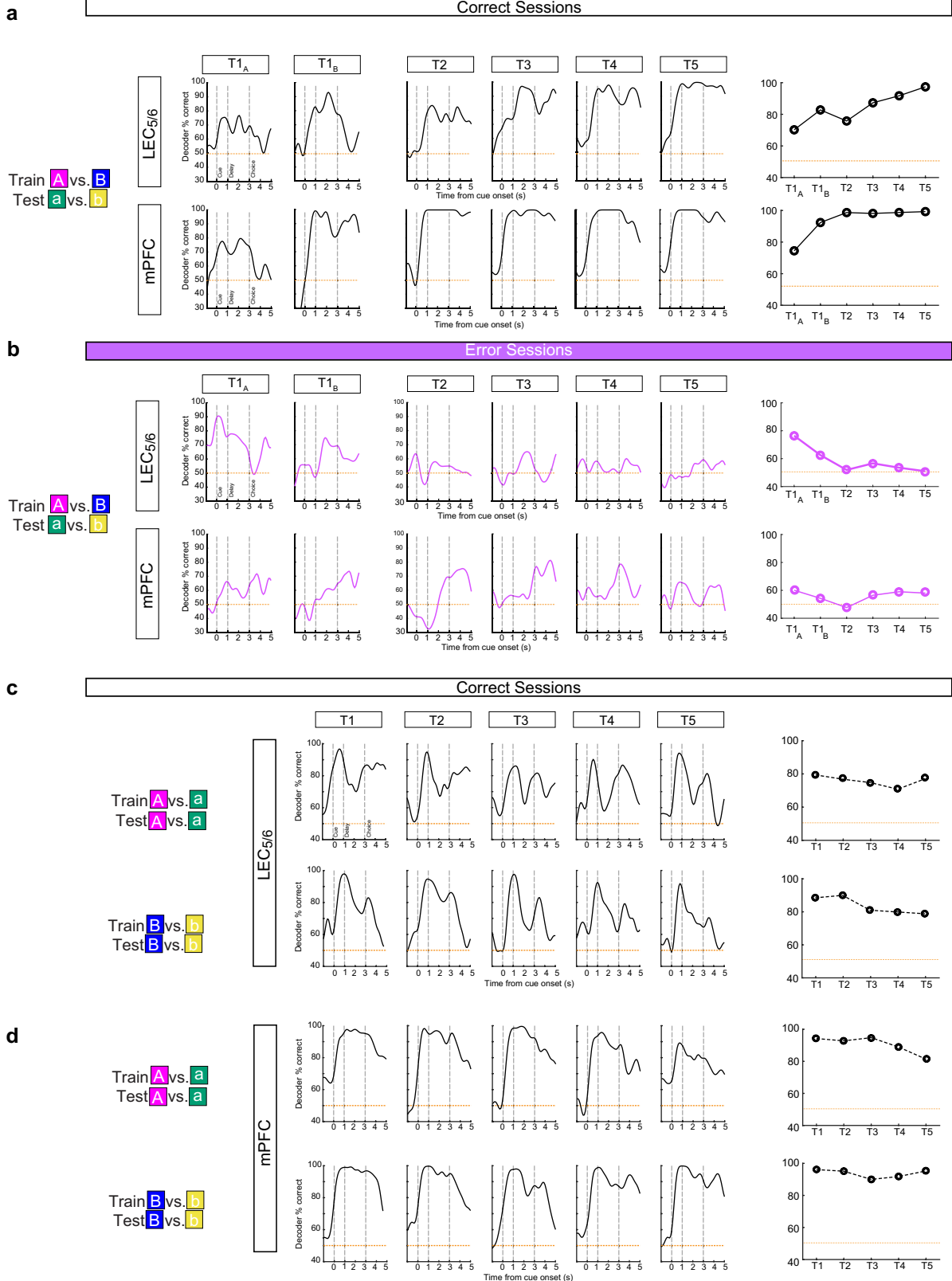
Odors A-a and between Odors B-b showed significant increase from T1 to T5 ($p = 0.012$, $p = 0.0095$, respectively). (Middle) In inhibition sessions, SI for all odor pairs did not show significant differences from T1 to T5 (Aa: $p = 0.41$, Bb: $p = 0.07$, AB: $p = 0.15$, ab: $p = 0.23$), confirming the impairment of outcome classification. (Bottom) Direct comparison between control and inhibition sessions confirmed the disappearance of similar representations between Odors-A and -a ($p = 0.0014$ at T5). * $p < 0.05$, ** $p < 0.01$, *** $p < 0.001$, two-sided bootstrapping test, n = 1000 bootstraps each. Data are presented as mean values +/- SEM.



Extended Data Fig. 19 | Fast development of odor outcome representation in mPFC population. (a) Development of task performance, Similarity Index (SI) between Odors-A and a (SIA-a) for LEC_{LS/6} cell population, and SI between

Odors B and b (SIB-b) for LEC_{LS/6} cell population. Variables are normalized onto a scale from 0 (T1a) to 1(T5). (b) Development of task performance, SIA-a for mPFC population and SIB-b for mPFC population as above.

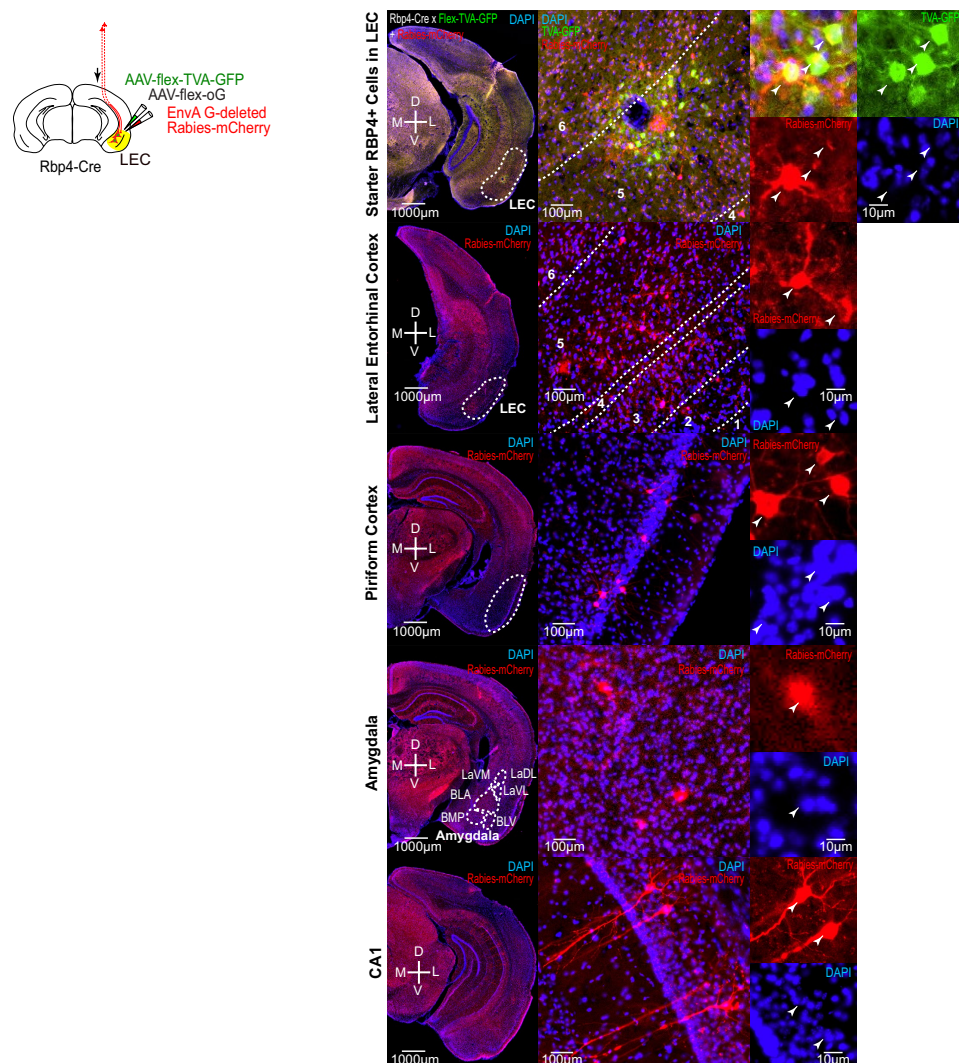
Article



Extended Data Fig. 20 | See next page for caption.

Extended Data Fig. 20 | Decoding analyses of LEC_{L5/6} and mPFC population activity. (a-b) A support vector machine (SVM) decoder was trained to discriminate novel Odor-a vs. Odor-b, using neural responses to familiar Odor-A vs. Odor-B in the same timepoint (T) as training data. For each 100 ms time bin, 100 SVMs were trained and their performances averaged to achieve the final % correct value. Decoding performance increases quickly in mPFC between T1-T2 (~90% at Trials 6-10 (T1b)), while performance only gradually reached ~90% at T3 in LEC_{L5/6}, indicating a quicker development of outcome representation in mPFC. T1_A= trials 1-5; T1_B= trials 6-10. **a)** Decoder performance for Correct sessions. (Top row) LEC_{L5/6} population. (Bottom row) mPFC population. Right: Average performance from the 0.5-3 s window of each timepoint. **b)** As above,

but for Error sessions. **(c-d)** The decoder was trained to discriminate within outcome categories (Odor-A vs. Odor-a OR Odor-B vs. Odor-b), using half the trials of one timepoint to train and the other half to test. Although the discriminatory power between Odor-A and Odor-a gradually decreased from T1 to T5, it remained at ~75% at T5. This result suggests that LEC neural activities still have information distinct enough for the decoder to discriminate between Odor-A and -a at T5. This was also the case for Odor-B vs Odor-b (78% at T5), as well as mPFC (82% at T5 for A vs a, 98% at T5 for B vs b). **(c)** Decoder performance for LEC_{L5/6} population during Correct sessions. **(d)** Decoder performance for mPFC population during Correct sessions.



Extended Data Fig. 21 | Characterizing monosynaptic input to *Rbp4*⁺ LEC_{L5/6} cells using retrograde rabies tracing. Monosynaptic retrograde tracing of *Rbp4*⁺ LEC_{L5/6} neurons. (Left) Cre-dependent glycoprotein and TVA-GFP virus (green) and G-deleted rabies virus expressing mCherry (red) were injected into the LEC_{L5/6} of *Rbp4*-Cre mice. (Right) Top panel shows coronal sections revealing starter *Rbp4*⁺ cells (indicated by white arrows) that are double positive (red and green) near the injection site. The remaining panels

demonstrate coronal sections with examples of presynaptically labelled neurons (red only) from local LEC, posterior piriform cortex, amygdala and hippocampal CA1 of the intermediate-ventral tiers (indicated by white arrows). (BLA = Basolateral amygdala, BMP = Basomedial posterior amygdala, BLV = Basolateral ventral amygdala, LaVL = Lateral amygdala ventrolateral, LaVM = Lateral amygdala ventromedial and LaDL = Lateral amygdala dorsolateral).

Reporting Summary

Nature Portfolio wishes to improve the reproducibility of the work that we publish. This form provides structure for consistency and transparency in reporting. For further information on Nature Portfolio policies, see our [Editorial Policies](#) and the [Editorial Policy Checklist](#).

Statistics

For all statistical analyses, confirm that the following items are present in the figure legend, table legend, main text, or Methods section.

n/a Confirmed

- The exact sample size (n) for each experimental group/condition, given as a discrete number and unit of measurement
- A statement on whether measurements were taken from distinct samples or whether the same sample was measured repeatedly
- The statistical test(s) used AND whether they are one- or two-sided
Only common tests should be described solely by name; describe more complex techniques in the Methods section.
- A description of all covariates tested
- A description of any assumptions or corrections, such as tests of normality and adjustment for multiple comparisons
- A full description of the statistical parameters including central tendency (e.g. means) or other basic estimates (e.g. regression coefficient) AND variation (e.g. standard deviation) or associated estimates of uncertainty (e.g. confidence intervals)
- For null hypothesis testing, the test statistic (e.g. F , t , r) with confidence intervals, effect sizes, degrees of freedom and P value noted
Give P values as exact values whenever suitable.
- For Bayesian analysis, information on the choice of priors and Markov chain Monte Carlo settings
- For hierarchical and complex designs, identification of the appropriate level for tests and full reporting of outcomes
- Estimates of effect sizes (e.g. Cohen's d , Pearson's r), indicating how they were calculated

Our web collection on [statistics for biologists](#) contains articles on many of the points above.

Software and code

Policy information about [availability of computer code](#)

Data collection Cheetah v 5.7.1 and v 6.1 (Neuralynx Inc)

Data analysis Matlab R2020a (Mathworks)

For manuscripts utilizing custom algorithms or software that are central to the research but not yet described in published literature, software must be made available to editors and reviewers. We strongly encourage code deposition in a community repository (e.g. GitHub). See the Nature Portfolio [guidelines for submitting code & software](#) for further information.

Data

Policy information about [availability of data](#)

All manuscripts must include a [data availability statement](#). This statement should provide the following information, where applicable:

- Accession codes, unique identifiers, or web links for publicly available datasets
- A description of any restrictions on data availability
- For clinical datasets or third party data, please ensure that the statement adheres to our [policy](#)

All data can be obtained from the corresponding author upon reasonable request.

Research involving human participants, their data, or biological material

Policy information about studies with [human participants or human data](#). See also policy information about [sex, gender \(identity/presentation\), and sexual orientation](#) and [race, ethnicity and racism](#).

| | |
|--------------------------------------------------------------------|-----------------------------------------|
| Reporting on sex and gender | <input type="checkbox"/> Not applicable |
| Reporting on race, ethnicity, or other socially relevant groupings | <input type="checkbox"/> Not applicable |
| Population characteristics | <input type="checkbox"/> Not applicable |
| Recruitment | <input type="checkbox"/> Not applicable |
| Ethics oversight | <input type="checkbox"/> Not applicable |

Note that full information on the approval of the study protocol must also be provided in the manuscript.

Field-specific reporting

Please select the one below that is the best fit for your research. If you are not sure, read the appropriate sections before making your selection.

Life sciences Behavioural & social sciences Ecological, evolutionary & environmental sciences

For a reference copy of the document with all sections, see nature.com/documents/nr-reporting-summary-flat.pdf

Life sciences study design

All studies must disclose on these points even when the disclosure is negative.

| | |
|-----------------|----------------------------------------------------------------------------------------------------------------------------------------------------------------------------------------------------------------------------------------------------------------------------------------------------------------------------------------------------------------------------------------|
| Sample size | No statistical method was used to pre-determine sample sizes, but we chose sample sizes that exceeded or matched those reported in previous studies with similar methodologies (Lee et al., Nature 2021). Both males and females were included in the samples. We did not find any difference between sexes, thus data from males and females were combined and reported in the study. |
| Data exclusions | Criteria for data exclusion based on lack of viral expression or mistargeting of injection/implantation were established prior to the experiments. Otherwise, no systematic data exclusion was performed. |
| Replication | The total number of animals and neurons is reported for all experiments in the statistical data summary sheet. Recording experiments were replicated across cohorts of mice allocated to recording only vs. recording plus inhibition experiments. Bootstrapping analyses address replication within neuronal population (see Methods). |
| Randomization | For all experiments mice were randomly assigned as to which implantation they received, the virus injection location and protocol used. |
| Blinding | Experimenters were blind to genotype, region targeted and optogenetic protocol in all experiments and analyses. |

Reporting for specific materials, systems and methods

We require information from authors about some types of materials, experimental systems and methods used in many studies. Here, indicate whether each material, system or method listed is relevant to your study. If you are not sure if a list item applies to your research, read the appropriate section before selecting a response.

| Materials & experimental systems | | Methods | |
|-------------------------------------|-----------------------------------------------------------------|-------------------------------------|-------------------------------------------------|
| n/a | Involved in the study | n/a | Involved in the study |
| <input checked="" type="checkbox"/> | <input type="checkbox"/> Antibodies | <input checked="" type="checkbox"/> | <input type="checkbox"/> ChIP-seq |
| <input checked="" type="checkbox"/> | <input type="checkbox"/> Eukaryotic cell lines | <input checked="" type="checkbox"/> | <input type="checkbox"/> Flow cytometry |
| <input checked="" type="checkbox"/> | <input type="checkbox"/> Palaeontology and archaeology | <input checked="" type="checkbox"/> | <input type="checkbox"/> MRI-based neuroimaging |
| <input type="checkbox"/> | <input checked="" type="checkbox"/> Animals and other organisms | | |
| <input checked="" type="checkbox"/> | <input type="checkbox"/> Clinical data | | |
| <input checked="" type="checkbox"/> | <input type="checkbox"/> Dual use research of concern | | |
| <input checked="" type="checkbox"/> | <input type="checkbox"/> Plants | | |

Animals and other research organisms

Policy information about [studies involving animals](#); [ARRIVE guidelines](#) recommended for reporting animal research, and [Sex and Gender in Research](#)

Laboratory animals

Rbp4-Cre mouse (MMRRC, 037128), C57BL/6J mouse (Jackson, 000664). Animals were used in 3–8 months of age. Both females and males were included (see animal summary sheet). See Methods for details of housing conditions.

Wild animals

No wild animals were used in the study.

Reporting on sex

Both males and females were included in the study. See summary table for sex of individual subjects. No difference between males and females was observed in preliminary analyses.

Field-collected samples

No field collected samples were used in the study.

Ethics oversight

Institutional Animal Care and Use Committee at the University of California, Irvine.

Note that full information on the approval of the study protocol must also be provided in the manuscript.

Plants

Seed stocks

Not applicable

Novel plant genotypes

Not applicable

Authentication

Not applicable